Paris, R., Ramalho, R. S., Madeira, J., Ávila, S., May, S. M., Rixhon, G., Engel, M., Brückner, H., Herzog, M., Schukraft, G., Perez-Torrado, F. J., Rodriguez-Gonzalez, A., Carracedo, J. C., & Giachetti, T. (2017). Mega-tsunami conglomerates and flank collapses of ocean island volcanoes. *Marine Geology*, *395*, 168-187. https://doi.org/10.1016/j.margeo.2017.10.004

Megatsunami conglomerates and flank collapses of ocean island volcanoes

Raphaël Paris[1], Ricardo S. Ramalho[2,3,4], José Madeira[3], Sérgio Ávila[5,6], Simon Matthias May[7], Gilles Rixhon[7], Max Engel[7], Helmut Brückner[7], Manuel Herzog[8], Gerd Schukraft[8], , Francisco José Perez-Torrado[9], Alejandro Rodriguez-Gonzales[9], Juan Carlos Carracedo[9], Thomas Giachetti[10]

[1] Université Clermont Auvergne, CNRS, IRD, OPGC, Laboratoire Magmas and Volcans, F-63000 Clermont-Ferrand, France (e-mail: raphael.paris@univ-bpclermont.fr).

[2] Instituto Dom Luiz, Faculdade de Ciencias, Universidade de Lisboa, 1749-016 Lisboa, Portugal

[3] School of Earth Sciences, University of Bristol, Wills Memorial Building, Queen's Road, Bristol BS8 1RJ, UK

[4] Lamont-Doherty Earth Observatory, Columbia University, Comer Geochemistry Building, PO Box 1000, Palisades, NY10964-8000, USA

[5] CIBIO, Centro de Investigação em Biodiversidade e Recursos Genéticos, InBIO Laboratório Associado, Pólo dos Açores, Azores, Portugal

[6] Departamento de Biologia, Universidade dos Açores, 9501-801 Ponta Delgada, Açores, Portugal

[7] Institute of Geography, University of Cologne, Albertus-Magnus-Platz, 50923 Cologne, Germany

[8] Institute of Geography, University of Heidelberg, 69120 Heidelberg, Germany

[9] Instituto de Estudios Ambientales y Recursos Naturales (i-UNAT),, Universidad de Las Palmas de Gran Canaria, 35017 Las Palmas de Gran Canaria, Spain

[10] Department of Earth Sciences, University of Oregon, Eugene, USA

Abstract

Keywords: tsunami; conglomerate; volcano instability; landslide; oceanic shield volcanoes; Hawaii; Canary Islands; Cape Verde Islands.

1. Introduction

Ocean island volcanoes experience rapid changes in morphology due to volcanism, subsidence or uplifting, flank instability, and erosion (e.g. Menard, 1983 andand 1986; Mitchell, 1998 andand 2003; Keating andand McGuire, 2000; Paris, 2002; Ramalho et al., 2013). Extreme-wave events such as storms and tsunamis are important agents of onshore-offshore sediment transport and play a key role in the evolution of volcanic islands (e.g. Johnson et al., 2017). Source mechanisms of tsunami impacting volcanic islands are varied: local or distant earthquakes, instabilities, eruptive processes (pyroclastic flows, underwater explosions, caldera collapse, etc.), and nuclear explosions. Among all these mechanisms, only large flank collapses have the potential to generate megatsunamis (Goff et al., 2014). The term "megatsunami" is commonly and often arbitrary used in the media, but Goff et al. (2014) proposed a definition based on the wave amplitude exceeding 50 m. Megatsunamis thus have a magnitude exceeding all published tsunami magnitude scales (e.g. Imamura, 1942; Iida 1963; Soloviev, 1972; Abe, 1979; Hatori, 1986). The 1958 tsunami in Lituya Bay (Miller, 1960) can be considered as the only historical example of megatsunami, but the maximum runup of 524 m was spatially limited to the slope opposite to the landslide (30.6×10^6 m³) and

rapidly decreased down to 10 m at 12 km from the source. Volcanic edifices are particularly prone to flank instability due to rapid growth, structural discontinuities, hydrothermal alteration, magma intrusions, and seismicity (e.g. Siebert, 1984; Carracedo, 1996; Van Wyk de Vries and Francis, 1997; Keating and McGuire, 2000; Lagmay et al., 2000; Quidelleur et al., 2008). Slope instabilities at volcanoes range from rockfalls and small landslides ($<10^6$ m³) to large debris avalanches (up to the order of 10^2 km³). Successive landslides of 17×10^6 m^3 and 5×10^6 m^3 on the flanks of Stromboli Island in December 2002 generated a local tsunami with a maximum runup of 8 m on the island itself, and limited effect on the coasts at a distance of more than 200 km (Maramai et al. 2005). The 5 km³ debris avalanche of Ritter Island in 1888 produced a large tsunami in all Bismarck Sea, with runups up to 15 m on the islands nearby, and 5 m at 500 km from the volcano (Cooke, 1981; Ward and Day, 2003). Mass wasting of ocean island volcanoes implies volumes of tens to hundreds of km³, as evidenced by mass transport deposits offshore and collapse scars onshore (e.g. Moore et al., 1989; Holcomb and Searle, 1991; Normark et al., 1993; Carracedo et al., 1999; Day et al., 1999; Masson et al., 2002, 2008; Mitchell, 2003; Oehler et al., 2004; Paris et al., 2005;). However, it is difficult to infer the mechanisms controlling these giant flank collapses and to evaluate tsunami hazards, because (1) we lack observational or instrumental data on such low-frequency, high magnitude events, (2) and the geological record of such events is often incomplete and difficult to interpret.

Here we present a review on the present-day knowledge of high-elevation fossiliferous conglomerates on ocean island volcanoes, which are attributed to the impact of megatsunamis triggered by volcano flank collapses. The paper is organised as follows. First, we present a brief review on elevated marine deposits that were widely debated in the literature (tsunami deposits or uplifted littorals?). Pioneering works in Hawaii inspired later studies in the Canary and Cape Verde Islands, as well as in the Indian Ocean (Reunion Island and Mauritius). The, we address the main problems affecting the identification, interpretation, and dating of megatsunami conglomerates.

2. The Hawaiian debate: elevated marine deposits as evidence of tsunami or uplifted littorals?

The interpretation of elevated marine deposits on the southern flanks of Lāna‘i and Moloka‘i is a long debate in Hawaii’s history of geology. The controversy started when Moore and

Moore (1984) proposed that the so-called Hulopoe Gravel (Lānaʻi), described by Stearns (1938, 1978) as an ancient littoral deposit, was in fact deposited by a "giant wave", i.e. a tsunami wave (Fig. 1). The tsunami hypothesis relies both on geophysical and sedimentological data. Moore and Moore (1984) presented the Hulopoe Gravel a single landward fining and thinning formation that originally blanketed the southern flanks of Lānaʻi at altitudes up to 326 m a.p.s.l. (above present sea level; altitude measured by Stearns, 1938). Note that the term "conglomerate" should be used rather than "gravel", since the deposits are cemented by calcrete. The great majority of the clasts are local basalts, but a marine origin is inferred from the presence of corals, beach-rock and molluscs. Skeletons of corals and other reef organisms are not in a growth position. Ten years later, Moore et al. (1994) described a similar marine conglomerate on the southern flank of Molokaʻi. Moore and Moore (1984) also argued that the south-eastern Hawaiian Islands subside too fast for preserving deposits of past sea-level highstands. The origin of the Hulopoe Gravel is in fact one of the key issues in controversies concerning the vertical motion of the south-eastern Hawaiian Islands (Webster et al., 2010). Tide gage records and drowned reefs around these islands indicate both historical and long-term subsidence (Moore, 1971, 1987; Moore and Fornari, 1984; Moore and Campbell, 1987; Ludwig et al., 1991; Wessel, 1993; Moore et al., 1996; Smith et al., 2002).

However, the tsunami hypothesis has been revisited by several authors. Increasing age of coralline beach deposits with elevation on Oʻahu and Molokaʻi together with observations of wave-cut notches and terraces are in favour of ancient shorelines uplifted (Brückner and Radtke, 1989; Grigg and Jones, 1997). Large uplift of oceanic shield volcanoes can be produced by lithospheric flexures (e.g. Watts and ten Brink, 1989; Grigg and Jones, 1997; Huppert et al., 2015), or alternatively by isostatic compensation (rebound) following large collapses (e.g. Smith and Wessel, 2000), or even by intrusive processes (e.g. Ramalho et al. 2010a, 2010b; Klügel et al., 2015; Ramalho et al. 2017). Detailed description of the lithofacies and biofacies of the Hulopoe Gravel allowed distinguishing distinct subunits and assemblages of littoral to sublittoral fauna separated by erosional discontinuities and palaeosols (Rubin et al., 2000; Felton, 2002; Felton et al., 2006; Crook and Felton, 2008). The sequence of elevated marine deposits would then represent unconformity-bounded cycles of transgressive and regressive facies surimposed on a longer-time scale flexural uplift (Felton et al., 2006), even if reworking of the deposits by tsunami or hurricane cannot entirely be ruled out (Felton et al., 2006; Crook and Felton, 2008). However, the chronology of drowned reefs

offshore Lāna‘i does not support the uplift hypothesis (Moore and Campbell, 1987; Webster et al., 2006, 2007, 2010). The controversy is also fuelled by coeval dating of coral clasts from the Lanai and Molokai deposits (Moore and Moore, 1988, 1994; Rubin et al., 2000) and the Alika 2 and South Kona landslides (Lipman et al., 1988; McMurtry et al., 1999) coincident with MIS (marine isotopic stages) 5e and 7. It is thus tempting to correlate the onset of interglacials with reinforced instability of the islands, favouring large flank collapses and tsunamis (e.g. McMurtry et al., 2004a). The debate remains open, while the key outcrop at 326 m a.p.s.l. on the southern flank of Lāna‘i was destroyed during the Second World War (Crook and Felton, 2008).

The marine fossiliferous conglomerate described by Stearns and McDonald (1946) on the western flank of Kohala volcano (northwest Hawaii), and later re-examined and dated 106-102 ka by McMurtry et al. (2004b), could finally represents the most convincing evidence of megatsunami in Hawaii. The Kohala peninsula has been subsiding for the last 475 ka (Campbell, 1984; Ludwig et al., 1991). Considering the present-day maximum elevation of the conglomerate (61 m a.p.s.l.) and the subsidence rate, a tsunami runup >400 m can be inferred (McMurtry et al. (2004b).

3. Canarian clues to the Hawaii megatsunami hypothesis

Unlike the Hawaiian Islands, the Canary Islands are not affected by long-term subsidence because plate motion over the mantle plume is slower and oceanic crust is more rigid (e.g. Carracedo et al., 1998). However, the growth of volcanic edifices on the flanks of each other over prolonged periods of time, from the shield building stages to rejuvenated stages, results in migrating lithospheric flexures and tilting of the islands, as evidenced by erosion rates (Ménendez et al., 2008) and elevated Mio-Pliocene and Quaternary littoral deposits (Zazo et al., 2002, 2003; Meco et al., 2007). Three marine conglomerates do not fit into the framework of relative sea-level changes and vertical movements in the Canary Islands, and display unusual sedimentary and palaeontological characteristics. They are described below.

3.1. The Agaete tsunami conglomerates, Gran Canaria

The first evidence of megatsunami in the Canary Islands was provided by Perez-Torrado et al. (2002, 2006), who interpreted a fossiliferous conglomerate on the north-western coast of Gran Canaria, Agaete valley (Fig. 2), as a tsunami deposit. The Agaete conglomerate was previously interpreted as a single palaeolittoral (e.g. Denizot, 1934; Lecointre et al., 1967; Klug, 1968; Meco, 1989), but it is in fact attached to the slopes of the valley at elevations ranging between 41 and 188 m a.s.l. (Perez-Torrado et al., 2006). The present-day outcrops of conglomerate are the remnants of a large deposit that initially fossilised the relief of the entire valley. Whatever the nature of the substratum (old lavas, soil, scree deposits), the basal contact is always erosive, showing rip-up clasts of soil up to 1 m large (Fig. 4C in Perez-Torrado et al., 2006) and downward-injected clastic dykes (Fig. 3A). The lithology of the clasts and the taphonomy of the fossiliferous content (bioclasts) point to a mixing of sublittoral, littoral, alluvial and colluvial sources. Molluscan fauna is typical of the Upper Pliocene and Pleistocene interglacial stages in this area (Meco, 1989, 2008; Meco et al., 2002). The marine bioclasts are never found in life position, and the shells of the bivalves are often separated and fragmented. The overall thickness of the conglomerate, and the size and roundness of the clasts decrease with altitude (Fig. 4). However, the thickest (and lowest) outcrops reveal that the tsunami conglomerate is internally stratified into distinct subunits with poor lateral continuity. Perez-Torrado et al. (2006) initially described two main subunits; the lower subunit being coarser, less sorted and less rich in bioclasts compared to the upper subunit (Fig. 4). The contact between the two subunits is characterised by scour-and-fill features. Cobble imbrication is mostly governed by the topography, but when the two subunits are present, the lower unit is preferentially landward-imbricated (tsunami uprush) whereas the upper subunit is seaward-imbricated (backwash) (Paris et al., 2004; Perez-Torrado et al., 2006). Real estate projects later revealed new sections, showing a more complete stratigraphy of the tsunami sequence. Madeira et al. (2011a) found another tsunami conglomerate below the one described by Perez-Torrado et al. (2006). The contact between the two tsunamis is characterised by the development of a palaeosol (Fig. 3B).

The succession of two tsunamis in the same valley during the Pleistocene is concordant with the recurrence of massive and sometimes multistage flank collapses in the Canary Islands (Watts and Masson, 2001; Masson et al., 2002; Paris et al., 2005; Giachetti et al., 2011; Hunt et al., 2001, 2013a). The most probable source of the Agaete megatsunami is the Güímar flank collapse on the eastern flank of Tenerife Island (Fig. 2). The scar of the landslide onshore has

a volume of 47 km³ (Paris et al., 2005). Numerical simulations of the collapse by Giachetti et al. (2011) demonstrate that a multistage scenario with five successive blocks generates a tsunami large enough to explain the spatial distribution of the tsunami deposits in the Agaete valley. Thus, a massive collapse of 47 km³ in one-go is not mandatory, even if this hypothesis is not ruled out. Without direct dating of the two Agaete tsunamis (< 1.75 Ma after Meco et al., 2002), it is actually difficult to better constrain the timing and scenario of the Güímar flank collapse (dated 860-830 ka by Carracedo et al., 2011), and to reconstruct accurately the tsunami runup relatively to coeval sea level.

3.2. The link with explosive volcanism: the Icod flank collapses and tsunamis, Tenerife

The formation and differentiation of shallow magmatic reservoirs in the central part of Tenerife Island (Las Cañadas edifice) is associated with recurrent ignimbrite-forming eruptions (e.g. Martí et al., 1994; Bryan et al., 1998; Ancochea et al., 1999; Brown et al., 2003; Edgar et al., 2007). Dávila Harris et al. (2011) suggested that one of these explosive eruptions generated a debris avalanche on the south-eastern flank of Tenerife 733 ky ago. The recent discovery of tsunami deposits on the north-western coast of Tenerife (Fig. 5: Ferrer et al., 2013; Coello Bravo et al., 2014; Paris et al., 2017) was the opportunity to revisit the debate on the origin of the Las Cañadas caldera and the possible link between explosion caldera and flank collapse.

As in Gran Canaria and Hawaii, the Tenerife tsunami deposit is a poorly sorted marine conglomerate fining landward. The biodiversity of the fauna of bivalves, gastropods, foraminiferas, calcareous algae, and coral fragments indicates a mixing of different environments, species of the infra-circalittoral zones being dominant (Coello Bravo et al., 2014; Paris et al., 2017). The maximum age for the tsunami units is inferred from the age of the youngest lava flows on which they stand (178 ka: Carracedo et al., 2007). The internal structure of the conglomerate differs from one site to another, but two main subunits can be distinguished (cf. fig. 3 in Paris et al., 2017). The lower subunit is mostly composed of local-derived basalts (i.e. coastal lava flows eroded by the tsunami) and its elevation never exceeds 20 m. The upper subunit incorporates phonolites, hydrothermally altered rocks, syenites, obsidian and pumices. This composition is similar to the Abrigo breccia, which corresponds

to the uppermost subunit of the Abrigo ignimbrite dated 175 ka (Martí et al., 1994; Pittari et al., 2006; Edgar et al., 2007; Boulesteix et al., 2012). The pumice clasts found in the upper tsunami subunit are clearly ascribed to the Abrigo eruption (Paris et al., 2017). The upper tsunami subunit thus inundated the north-western coasts of Tenerife at elevations up to 132 m (Fig. 5) and incorporated freshly ejected pumices from the coeval Abrigo eruption. What caused these two successive tsunamis before and during a major explosive eruption?

Paris et al. (2017) proposed a scenario linking the two tsunamis, the Abrigo eruption, and the 175-165 ka Icod collapse on the northern flank of Tenerife (Watts and Masson, 1995, 2001; Ablay and Hürlimann, 2000; Masson et al., 2002; Wynn et al., 2002; Frenz et al., 2009; Hunt et al., 2011). The Icod collapse was a retrogressive event that mobilised a volume of ~200 km³ as recorded offshore by three debris lobes and seven turbidites (Hunt et al., 2011). Juvenile glass of the Abrigo eruption appears only in the last turbidite. Paris et al. (2017) argued that the first tsunami was generated during the submarine stage of the retrogressive failure and before the onset of the Abrigo eruption, whereas the second and larger tsunami followed the debris avalanche of the subaerial edifice and emplacement of the Abrigo breccia. This original scenario of coupled explosive eruption and flank collapse represents a new type of volcano-tectonic event on oceanic shield volcanoes.

3.3. Another evidence of the Icod megatsunami in Lanzarote?

The south and south-western coasts of Lanzarote are draped by several levels of Quaternary marine terraces at elevations up to 70 m (e.g. Driscoll et al., 1965; Meco and Sterans, 1981; Zazo et al., 2002). Zazo et al. (2002) distinguished six marine terraces between +0.5 and +25 m a.s.l. lying on lava flows dated to 1.2 Ma (Montaña Roja). The +8-10 m terrace is a coarse fossiliferous conglomerate interbedded between Montaña Roja and Montaña de Femés lava flows (160 ka: Zazo et al., 2002). Basaltic boulders up to 1.5 m are embedded in a coarse sand-to-pebble matrix (Fig. 6). A palaeodune and a palaeosol are intercalated between the conglomerate and the Montaña Roja lavas. Meco (2008) describes the sequence of marine terraces located between +8 and +25 m as a single tsunami deposit. His main argument is that the interglacial molluscan fauna of the conglomerate represents a mixing of terrestrial, littoral (intertidal), infralittoral and circalittoral species, which are never observed in life position.

The age of the marine conglomerate is poorly constrained (1200-160 ka), but Meco (2008) considered MIS 9.3 as a likely candidate. However, the hypothesis of a MIS7 (243-191 ka: Lisiecki and Raymo, 2005) fauna later reworked by a tsunami cannot be discarded and would be compatible with the age of the Icod event (175-165 ka).

3.4. Far-field tsunami conglomerates related to flank collapse in the Canary Islands

The potential far-field impact of megatsunamis triggered by flank collapses of the Canary Islands has been debated on the basis of numerical simulations (e.g. Ward and Day, 2003; Løvholt et al., 2008; Abadie et al., 2012). Far-field sedimentary records of such events are rare. On the north-eastern Bermuda platform, the origin of a marine conglomerate has been vividly debated and was either associated with a megatsunami (McMurtry et al., 2007) or a +21 m sea-level highstand of MIS 11 (Olson and Hearty, 2009). More investigations are needed, particularly on the eastern coasts of the Lesser Antilles Islands and western coast of Africa, in order to document the far-field impact of Canarian megatsunamis.

4. Tsunami deposits of the Cape Verde Islands

4.1. The Tarrafal tsunami conglomerate and megaclasts, Santiago Island

The identification of megatsunami deposits in Hawaii and the Canary Islands stimulated the search for similar evidence in the Cape Verde Islands. Following the criteria for identifying tsunami deposits in rocky coast environments such as Hawaii and the Canary Islands, Paris et al. (2011) found convincing evidence of tsunami on the north-western coast of Santiago Island (Fig. 7). Despite its relatively low present-day elevation (6-12 m a.p.s.l.), the conglomerate described by Paris et al. (2011) displays all the diagnostic criteria proposed by earlier studies (Fig. 8): heterogeneous composition of local-derived volcanic rocks and marine fossils (never in life position) cemented by calcrete, erosive base (scour-and-fill features) and rip-up clasts of the underlying substratum, downward-injected veins of the conglomerates

(clastic dykes) inside the palaeosol, complex internal organisation with a poor lateral continuity of the subunits (five sedimentary facies are distinguished), lenticular bedding, poor sorting, frequent inverse grading, both landward and seaward imbrication of the clasts (when preserved). These characteristics allowed distinguishing the tsunami deposits from other uplifted littoral deposits observed on the coasts of Santiago Island (Lecointre, 1963; Serralheiro, 1976). Indeed, Ramalho et al. (2010a) estimated that Santiago Island has undergone a nearly-linear uplift of ~100 m/Ma during the last 4 Ma. At Tarrafal locality, the tsunami conglomerate is exposed along coastal cliffs, but its upward extension and thickness variation were inferred from Electrical Resistivity Tomography (ERT: Fig. 9).

Ramalho et al. (2015) later documented other outcrops of tsunami conglomerate and bioclastic sand at elevations up to 100 m a.s.l. on the northern and north-eastern coasts of Santiago (Fig. 7: Ribeira Funda, Angra). The sequences described by Ramalho et al. (2015) typically comprise one to three diffuse layers of extremely poorly sorted, matrix-supported conglomerates, with poor lateral continuity, and often exhibiting landward imbrication. Clasts range from small pebbles to metric basaltic boulders, either well-rounded or angular. Individual basaltic clasts may reach up to several meters in diameter, and rarely rest on the erosive base, being completely supported by the matrix. Rip-up clasts of soil and of friable tuffs can frequently be found embedded in the lower part of the deposits, typically within a calcarenite matrix. The topmost layer typically corresponds to a bioclastic-rich coarse sand sheet, which thins and fines landward, and exhibits a faint, undulating stratification. The proportion of marine bioclasts decreases landward, whereas the terrigenous contribution increases (Ramalho et al., 2015).

Preliminary analysis of the fauna indicates the abundant presence of fragments of corals, rhodoliths, molluscs (at least 15 taxa of bivalves and 96 taxa of gastropods), bryozoans and spines of echinoderms, as described for other tsunami deposits (Perez-Torrado et al., 2006; Paris et al., 2011; Coello Bravo et al., 2014). Moreover, all the shells of bivalves were disarticulated, and most of them were fragmented. The palaeobiodiversity of the tsunami deposit (111 taxa in one 1.5 kg sample) is very rich compared to the marine taxa of interglacial deposits (e.g. 143 fossil marine taxa reported from the Last Interglacial MIS 5e deposits of Santa Maria Island, Azores archipelago, collected along >10 years of research and in >300 samples: Ávila et al., 2015 and references therein). The mixture of taxa with different bathymetrical ecological zonation (shallow- and deep-water species), different life habits (epifaunal, infaunal, semi-infaunal, nektonic), and different types of substrate (rock, gravel,

sand, mud, algae, calcareous algae, corals) is also typical of tsunami deposits (e.g. Massari et al., 2009; Coello Bravo et al., 2014; Paris et al., 2017).In addition to the conglomerates, Ramalho et al. (2015) reported fields of megaclasts, which were quarried from a scarp edge (presently at 160-190 m a.p.s.l.)and transported upwards by the tsunami at elevations up to 220 m a.p.s.l. and 650 m from their source (Fig. 7: tsunami boulders). The megaclasts and the scarp have similar lithologies (submarine sheet flows, tufs and limestones). They are thus clearly allochtonous compared to the subaerial lavas on which they strand. Considering the dimensions of the largest basaltic boulder (9.4×6.8×3.8 m) and using the equations of Nandasena et al. (2011), the flow velocity required to initiate the transport ranges between 13 and 28 m/s depending on the pre-transport conditions (megaclast already detached from the scarp or joint-bounded). Without any constraint on the flow condition (e.g. subcritical or supercritical), it is difficult to estimate the flow depth inland after its minimum velocity. Numerical simulations of the Monte Amarelo collapse and tsunami (Paris et al., 2011) show that, whatever the rheology of the sliding mass (Mohr-Coulomb frictional rheology or plastic rheology), a multistage retrogressive failure generates a tsunami that inundate the Tarrafal peninsula at elevations up to 250 m a.p.s.l. (Fig. 10). Assuming Froude numbers $0.75<Fr<1.5$ (which correspond to the typical range for tsunami flows inland, cf. Matsutomi et al., 2011), the simulated flow depths are concordant with flow velocities estimated from the size of the boulders.

4.2. Age and source of the Tarrafal megatsunami

The western coast of Santiago Island is located in front of the active volcano of Fogo Island (Fig. 7). The eastern flank of Fogo collapsed during the Late Pleistocene, thus forming an 8 km-wide horseshoe-shaped caldera opened to the East and a massive debris avalanche deposit in the strait between Fogo and Santiago (Monte Amarelo collapse: Day et al., 1999; Le Bas et al., 2007; Masson et al., 2008). The estimated volume of the Monte Amarelo collapse (130-160 km^3) is roughly similar to the Icod collapse in Tenerife, but its morphology suggests a massive emplacement rather than multi-stage (Le Bas et al., 2007). The age of the Monte Amarelo collapse is locally bracketed by ^{3}He exposure ages of late pre-collapse (123 ka) and early post-collapse (62 ka) lava flows at Fogo (Foeken et al., 2009). Unpublished K-Ar and Ar-Ar ages of lava flows will soon provide a better estimate of the age of the collapse (Cornu

et al., 2017).There is actually a good agreement between the age of the collapse on Fogo and the age of the tsunami deposits on Santiago. Paris et al. (2011) obtained a ^{230}Th/U 230Th/U age of 123.6 ± 3.9 ka on a coral branch of the tsunami conglomerate. 230Th/U This age represents a maximum age for the tsunami, since the fossil corals might come from interglacial colonies reworked by the tsunami. Accordingly, Ramalho et al. (2015) estimated ^{3}He exposure ages of the tsunami megaclasts between 65.1 ± 1.9 and 84.0 ± 2.3 ka, with a mean arithmetic age of 73.3 ± 6.8 ka (Fig. 11).

4.3. Recurrent tsunamis on the coast of Maio Island

Marine conglomerates occur all around the coast of Maio (Madeira et al., 2011b). Stratigraphically, these deposits are covered by Upper Pleistocene fossil dunes and beach gravel, or Holocene deposits (alluvial, beach, dune, and salt flats in the western littoral). The conglomerates partly mantle the topography up to 5 km inland, ranging in elevation from present sea level to 40 m a.p.s.l. The basal contact with the substratum (palaeosol or alluvian fans) is sharp and erosive, showing rip-up clasts of the substratum. At some outcrops, sandstone with undulating bedding can be found either above or below the conglomerate (with floating boulders supported by the sand layer). On the eastern coast, Madeira et al. (2011b) distinguished up to three distinct conglomerates separated by colluvial deposits. The sequence has a cumulated thickness of up to 3 m. ^{230}Th/U ages on corals suggest that the third conglomerate could represent another evidence of the megatsunami generated by the flank collapse of Fogo ~70 ka ago (Madeira et al., 2017).

The conglomerates have a bimodal granulometry. The coarse fractions of angular-to-rounded boulders and cobbles cohabit with a medium-to-coarse bioclastic sand matrix. The texture is either matrix- or clast-supported depending on clast/matrix proportion. Clasts include all lithologies cropping out nearby (basalt, gabbro, limestone, marl, calcarenite, mudstone, and sandstone). Coarse clasts imbrication indicates both landward and seaward paleocurrents, representing influx and outwash. The matrix sand is cemented by secondary sparitic calcite. The macro-fossil fauna is very rich and abundant: rhodoliths, coral fragments, mollusc shells (including bivalves not in life position), and echinoderms from shallow littoral environment. Rounded clasts of calcareous algae represent the dominant population of bioclasts found in

the matrix, but foraminifers, although not abundant, are also present. These characteristics are similar to those of tsunami conglomerates described in Santiago (Paris et al., 2011; Ramalho et al., 2015) and Gran Canaria (Perez-Torrado et al., 2006)

5. Reunion Island and the Mauritius tsunami ca. 4500 ka

With more than 40 flanks collapses identified during the last 2 Ma (Labazuy 1996, Oehler et al., 2004), the Piton des Neiges and Piton de la Fournaise shield volcanoes at Réunion Island represent a significant source of tsunamis in the Indian Ocean. The last major flank collapse of Piton de la Fournaise volcano may have occurred ca. 4500 years ago (Bachèlery and Mairine, 1990; Labazuy, 1996). Numerical simulations show that a 10 km³ collapse on the eastern flank of Piton de la Fournaise volcano would generate waves up to 80 m high on the southern coast of Mauritius Island, located 170 km ENE of Réunion Island (Kelfoun et al., 2010).

Reef megaclasts at unusual elevations (3-40 m) for marine deposits (i.e. not linked to sea-level highstands) were described by Montaggioni (1978) along the coasts of Mauritius and Rodrigues islands. Uncalibrated ^{14}C and $^{230}Th/U$ ages of these blocks range between 3730 ± 100 BP and 6200 ± 800 BP (Montaggioni 1978). The hypothesis of old reefs partly eroded conflicts with the diversity of the sedimentary facies observed and the random orientation of the blocks (e.g. overturned, not in growth position). Most of the reef megaclasts are located between 3 and 15 m, but Montaggioni (1978) also mentioned an isolated 2 m³ *Porites* clast at 40 m a.p.s.l. on the northern coast. The largest megaclast (100 m³) was found at 4 m a.p.s.l. near Tamarin (western coast). Paris et al. (2013) later identified a tsunami conglomerate at 10-15 m a.s.l. on the southern coast of Mauritius (Fig. 12). The conglomerate is intercalated in a reddish lateritic soil at a depth of -50 to -80 cm. Preserved thickness of the conglomerate ranges between 20 and 45 cm and rapidly decreases landward as for the grain size. It is very poorly sorted and its composition reflects a mixing of two sediment sources: (1) marine bioclasts such as debris of corals (branching forms and brain corals), gastropods, and fragments of shells, and (2) fragments of locally-derived volcanic rocks and minerals, from sand-size to pebbles. The maximum age of the tsunami is given by a calibrated ^{14}C age of 4425 ± 35 BP on a coral branch (Paris et al., 2013). While there is no published sedimentary

evidence of tsunami at Réunion Island, a preliminary survey revealed a ridge of basaltic megaclasts up to 2 m large mixed with rounded pebbles overtopping dune deposits on the south-western coast, between Etang-Salé and Saint Louis (Fig. 13).

6. Discussion

6.1. Characteristics of megatsunami conglomerates

The megatsunami deposits described above fall in the category of conglomerates (and fields of boulders in the case of Tarrafal). The panel of methods used to characterise tsunami conglomerates is limited because of their coarse texture, so that methods used on sand-dominated tsunami deposits (e.g. textural and geochemical analyses on cores) cannot be applied. The extremely large grain size ratio (from clay to plurimetric boulder) makes the estimation of a total grain size distribution challenging. Horizontal and vertical trends of grain size can be inferred from *in situ* measurements or image analysis of the coarsest fractions only (coarse pebbles to boulders), and the structure and the bedforms are often difficult to identify. Consequently, the Hawaiian controversy shows that the distinction between tsunami conglomerates and other types of coarse-grained deposits (alluvial fan, pebble beach, storm ridge, etc.) is often problematic, especially in a rocky shore setting (e.g. Engel and May, 2012). However, tsunami conglomerates share a couple of characteristics with well-documented finer-grained tsunami deposits (e.g. Shiki and Yamazaki, 1996; Le Roux et al., 2004; Cantalamessa and Di Celma, 2005; Le Roux and Vargas, 2005; Perez-Torrado et al., 2006; Paris et al., 2011).

The sedimentological criteria used for identifying tsunami conglomerates are summarised in Table 1. Elevation alone is not a reliable criterion, because tsunami deposits might be preserved at elevations within the range of sea-level changes and marine terraces. Furthermore, elevation of the deposits needs to be corrected for later vertical movements of the island, using available uplift or subsidence rates. Elevated littoral deposits usually display distinct sedimentary facies that reflect the succession of different littoral zones or habitats. A tsunami deposit, in contrast, is a mixing of different sources of sediments redistributed both

inland and offshore. Tsunami conglomerates are typically attached to the topography and preserved as patches (lenticular geometry) at different elevations (Fig. 2), whereas marine deposits typically show great lateral continuity along elevated terraces on low-angle slopes.

Most of not all tsunami conglomerates described so far are internally organised in subunits, with erosional discontinuities between subunits (e.g. scour-and-fill structures on fig 4d in Perez-Torrado et al., 2006). However, this structure is often poorly-defined and subunits have a poor lateral continuity (Fig. 9 in Paris et al., 2011). Both fining and coarsening upwards sequence occur, depending on the wave scenario at a given locality. In some cases (e.g. Perez-Torrado et al., 2006), two well-defined subunits can be distinguished (Fig. 4): the coarse lower subunit displays landward clast fabric (uprush phase) and the finer upper subunit displays seaward clast fabric (backwash phase). The characterisation of bedding in conglomerates is not easy, but crude plane bedding and cross-lamination can develop in fine-grained facies.

Different trends of vertical grading are observed, inverse grading being frequent especially at the base of the lower subunits (Fig. 4). In terms of mean grain size and thickness, landward fining and thinning is considered as a key feature of tsunami deposits, including tsunami conglomerates (Fig. 4), even if it is often difficult to evaluate because of limited preservation and exposure. The opposite trend (landward thickening and coarsening) can be found when the deposits are trapped at the foot of steep slopes. Sorting of the clasts size ranges from moderately to very poorly sorted (Table 1). The majority of the facies are poorly sorted and clast-supported, but matrix-supported facies are observed in the upper part of some sequences (Cantalamessa and Di Celma, 2005). Matrix-supported facies are frequent when large quantities of fine marine and littoral sediments are available for transport by the incoming tsunami waves. As for the coarse size fractions (pebbles to boulders), the heterogeneous matrix reflects the different sources of fine-grained sediments mixed within the tsunami (beach, dune, marshes, etc.). A decreasing degree of clast roundness and flatness landward results from increasing abundance of angular clasts coming from supra-littoral slopes. The submerged position of the clasts prior to tsunami can be inferred from the presence of Lithophaga borings and biogenic incrustations such as vermetids and coralline algae (Fig. 8B).

The lower contact of tsunami conglomerates is erosive (Table 1), as evidenced by erosional features such as truncations of prominent features of the substratum (e.g. dykes in volcanic

setting) and rip-up clasts near the base of the deposit (e.g. rip-up clasts of soil). Intense shearing and a high pressure gradient at the base of the flow can lead to the formation of a traction carpet and downward clastic dykes injected in the substratum (Fig. 3A). The traction carpet is often cemented by calcrete and finer-grained than the overlying conglomerate (Fig. 14). X-ray microtomography revealed the existence of similar traction carpets in a finer-grained (clay-to-sand) historical tsunami deposit (Falvard and Paris, 2016; May et al., 2016).

The megatsunami conglomerates described in Hawaii, the Canary and Cape Verde Islands are partially cemented by a discontinuous calcrete ocaliche (Moore et al., 1984 and 1994; Perez-Torrado et al., 2006; Paris et al., 2011) that is more developed in the lower part of the deposits (Fig. 3B). At the base of the conglomerate, calcrete veins fill cracks and joints of the substratum (the veins are typically less than 1 m long and 5 mm large). Paris et al. (2011) distinguished two phases of cementation: (1) a first, rapidly-formed micritic gangue (microcristalline calcite) draping the clasts; (2) and a secondary, long-lasting but incomplete cementation by interstitial microsparite. Paris et al. (2011) proposed that the micritic gangue was formed from marine algae pulverized in the tsunami flow, the microsparite resulting from post-tsunami dissolution of the bioclasts.

Many of the aforementioned criteria might apply to other kinds of coarse-grained debris flows. Thus, the tsunami diagnostic relies specifically on three criteria (and is particularly true when associated with the other ones): (1) the succession of landward and seaward clast imbrication in the same sequence (Fig. 4); (2) the increasing abundance of terrestrial material upward and landward; (3) and the mixed and unusually rich fauna, ranging from terrestrial to circalittoral species (Table 1).

The subaqueous sedimentary density flow that occurred during the backwash of the 2004 tsunami in Sumatra (Paris et al., 2010) represent a modern analogue of tsunami conglomerate. The density flow was captured in a Spot-2 image and subsequent debris flow deposits were imaged by side-scan sonar images (Paris et al., 2010). Feldens et al. (2012) observed stiff mud deposits with grass, woods and shells transported by density flows in channels parallel to the 2004 tsunami backwash in Thailand. However, these observations lack the vertical dimension and structure of the deposits. The lobe-shaped debris flow deposit documented by Paris et al. (2010) covers an area of 3.5 km² (thickness could not be estimated). Side-scan sonar images show high concentrations of debris (boulders up to 9 m large, anthropogenic debris, tree

trunks) and the boulders are significantly coarser at the front and edges of the deposit (Fig. 5 in Paris et al., 2010).

6.2. Dating methods

Dating the time of tsunami deposition is crucial for reconstructing magnitude-frequency relationships and, in particular, recurrence rates of past tsunamis. For tsunamis induced by mass wasting events of volcanic edifices this in turn also implies chronological information on the volcanic collapse itself, which is particularly important for deciphering scenarios of inundation and relation to sea level (Fig. 11). Whilst young, fine-grained deposits in stratigraphic contexts can often be reliably dated by ^{14}C or optically stimulated luminescence (OSL - e.g. Cisternas et al., 2005; Brill et al., 2012), chronologies for the transport and deposition of supratidal coarse-clast sediments, such as tsunami conglomerates, are difficult to obtain.

Provided that the reservoir effect of the dated organisms can be determined, ^{14}C dating can yield reliable ages for the last 40-50 ka (Barbano et al., 2010). However, most deposits discussed here are too old for this method. If not, as in the case of Mauritius tsunami conglomerate (Paris et al., 2013), potential age overestimation through (multiple) post-mortem relocation of the dated material (i.e., corals, marine organisms attached to the clasts) must be considered, which may lead to a large age scatter as well (Suzuki et al., 2008). ^{14}C ages of boring bivalves may also considerably overestimate the timing of boulder transport due to post-mortem carbonate dissolution, recrystallization and replacement, i.e. neomorphism (Rixhon et al., 2017a).

When applicable, luminescence dating techniques (such as OSL and infrared stimulated luminescence - IRSL) are capable of extending chronologies back to the late and middle Pleistocene, with typical maximum age ranges of 150 ka for quartz and ~300 ka for feldspar (Rixhon et al., 2017b). Further methodological developments may even extend the datable range to Quaternary times scales (Roberts et al., 2015). However, very poorly sorted marine deposits may suffer from high dose scatter due to dose-rate heterogeneity, partial bleaching and sediment mixing (Sanderson and Murphy, 2010; Brill et al., 2017a). Although at an experimental state, OSL surface exposure dating of clasts may yield direct depositional ages

for boulder transport (Brill et al., 2017b). This approach is based on the measurement of the depth-dependent resetting of luminescence signals in exposed rock surfaces, which is compared to the signal-depth profiles of known-age samples (Sohbati et al., 2012a,b). Likewise, burial dating of pebble and cobble surfaces sampled from tsunami conglomerates using luminescence dating techniques may represent a useful alternative (Simms et al., 2011, 2012), although only few studies have successfully applied this approach to date.

^{230}Th /U dating represents the most common approach to estimate the age of poorly sorted marine deposits onshore, including megatsunami conglomerates (Moore and Moore, 1988; Moore et al., 1994; Rubin et al., 2000; McMurtry et al., 2004b; Paris et al., 2011). On the one hand, ^{230}Th/U dating of corals or attached organisms on boulders provides maximum ages but may likewise suffer from the reworking problem (Scheffers et al., 2014). On the other hand, ^{230}Th/U dating of secondary calcite precipitation occurring on tsunamigenic boulders in reef settings, such as flowstones or microbialites, yields reliable minimum ages, provided that carbonate precipitation can unambiguously be interpreted as post-depositional, and carbonate precipitation took place shortly after the transport event (Rixhon et al., 2017a). The same would theoretically hold for post-depositional calcrete formation in megatsunami deposits (Paris et al., 2011), but U-series isochron dating of such impure carbonates remains a methodological challenge (Candy et al., 2005).

Surface exposure dating based on concentration measurements of in situ-produced cosmogenic nuclides represents a promising approach for constraining the age of tsunami deposits (Ramalho et al., 2015; Rixhon et al., 2017a). Since basaltic clasts dominate the petrographic composition of tsunami conglomerates on the flanks of oceanic shield volcanoes, measuring ^{3}He in olivine crystals is recommended (Ramalho et al., 2015). In reef settings, ^{36}Cl measured in coralline calcite represents a useful alternative, although age accuracy strongly depends, amongst other issues, on the stable chlorine content in the coral samples (Rixhon et al., 2017a). Surface exposure dating may allow the combined dating of the volcanic flank collapse and the resulting megatsunami deposits. For instance, ^{3}He surface exposure ages of pre-and post-collapse lavas on Fogo Island bracket the Monte Amarello collapse (Foeken et al., 2009) and can be compared to ^{3}He surface exposure ages of tsunami megaclasts on northern Santiago Island (Fig. 11; Ramalho et al., 2015). Whilst post-emplacement processes and inheritance may induce an age scatter between individual boulders (e.g. inherited exposure at the source location of the clasts), the approach developed

by Rixhon et al. (2017a) for overturned tsunami boulders takes this potential bias into account.

6.3. Combining sedimentology and numerical models

The characteristics of tsunamis generated by landslidesdepend upon the initial geometry of the sliding mass (aspect ratio, thickness, volume), its origin (subaerial or submerged) and dynamical parameters (initial acceleration, maximum velocity, retrogressive behaviour, rheology) (e.g. Løvholt et al., 2015; Yavari-Ramshe and Ataie-Ashtiani, 2016). The diversity of the source parameters lead to the formation of different wave forms, such as Stokes, cnoidal, solitary or bore-like waves. Submarine flank collapses typically generate three main waves: (1) a crest propagating seaward (ahead of the slide front); (2) a large through propagating both shoreward and seaward; (3) and a second crest following the trough. The entrance of a subaerial collapse in water implies more complex processes in the splash zone, where different phases interact (fragments of rock and soil, ambient air and water), thus complicating the numerical simulations (e.g. Abadie et al., 2010; Di Risio et al., 2011). Note that the landslide itself is already multiphased (including interstitial fluid). Landslide time history and deformation offshore also influence the characteristics of the tsunami. Different conceptual models are used. The simplest approach is to model the effect of the landslide as an initial water surface condition (e.g. Synolakis et al., 1997). A more sophisticated approach couples the landslide motion and water volume displacement, the landslide being considered as rigid block (e.g. Ward and Day, 2001) or deformable mass having different rheologies (e.g. Fernández-Nieto et al., 2008; Kelfoun et al., 2010). Wave propagation is modelled using different equations, the mostly commonly used being (1) the non-dispersive linear or non-linear shallow-water equations (depth-averaged); (2) the dispersive non-linear Boussinesq models (depth-averaged); (3) the full Navier-Stokes equations (fully dispersive, three-dimensional), (4) or their simplified Reynolds-averaged version (Yavari-Ramshe and Ataie-Ashtiani, 2016, and references therein). The full Navier-Stokes equations are the best solution for a reliable simulation of landslide tsunamis (and particularly subaerial landslide), but they have a high computational cost.

The parameterisation of numerical simulations of tsunamis generated by large-scale flank collapses of ocean islands is delicate because we lack instrumental and observational data. The initial geometry of the collapse can be inferred from palaeotopographic reconstructions and geophysical surveys, but the dynamical parameters are poorly constrained (Paris et al., 2005). Information on flow dynamics can be retrieved from the morphology of the offshore deposits (aspect ratio, number of lobes, longitudinal and lateral levees, ridges, geometry of the front, spatial distribution of the hummocks, etc.). However, uncertainty on the collapse mechanisms (e.g. massive or multistage collapse) casts doubt on the validity of numerical simulations. It has been demonstrated that the rheology has a minor effect on the characteristics of the tsunami, compared to uncertainties on collapse mechanisms (Fig. 10). Assuming a multistage retrogressive behaviour for both the Monte Amarelo and Güímar collapse, numerical simulations of the tsunami runup are able to reproduce the spatial distribution of tsunami deposits, whereas massive collapses (in one-go) tend to overestimate the tsunami runup (Giachetti et al., 2011; Paris et al., 2011). The multistage nature of some flank collapses is also evidenced by the stratigraphy and composition of their distal turbidites, both in the Canary Islands (Hunt et al., 2011, 2013a) and Hawaiian Islands (Garcia, 1996). In the Canary Islands, the Icod collapse (see section 3.2) is recorded by three successive debris flows on the northern submarine flank of Tenerife (Watts and Masson, 2001), and a stacked sequence of seven turbidite subunits off northwest Africa (Hunt et al., 2011). The composition of the successive turbidite subunits suggests that the retrogressive failure affected successively the submarine flank of the island and the basaltic shield, and then the phonolitic-trachytic series of the Las Cañadas subaerial edifice. The scenario proposed by Hunt et al. (2011) is concordant with the structure and composition of the tsunami deposits on the north-western coast of Tenerife (Paris et al., 2017). Numerical simulations show that a 41 km³ submarine collapse generates tsunami waves high enough to submerge the coast until the maximum elevation of the first tsunami subunit (~50 m a.p.s.l.). A final 12 km³ en masse collapse of the subaerial edifice is required to explain the higher elevation reached by the second tsunami subunit (up to 132 m a.p.s.l.).

6.4. Links between volcanism, flank instability, and climate

Large-scale mass wasting of ocean islands is the result of a complex interplay between intrusive and eruptive processes, the structure of the edifice itself (discontinuities, weak

layers), and its environment (climate and sea level changes). The influence of external vs. internal parameters is still debated (e.g. Keating and McGuire, 2000; Mitchell, 2003; McMurtry et al., 2004a; Quidelleur et al., 2008; Hunt et al., 2013b, 2014; Coussens et al., 2016). The links between the instability of the volcanic edifice and the intrusive system are unambiguous, and possible mechanisms and feedbacks have been widely discussed (e.g. Carracedo, 1996; Day et al., 1999; Walter & Troll, 2003; Walter et al., 2005; Manconi et al., 2009; Delcamp et al., 2011; Cayol et al., 2014; Berthod et al., 2016). The formation of shallow magmatic reservoirs might also influence the destabilization of the upper part of the volcano (Amelung & Day, 2002). In the Canary Islands, the flank collapses are often preceded by periods of increasing rates of lava accumulation (Guillou et al., 1996; Paris, 2002; Carracedo et al., 2011).

On the other hand, McMurtry et al. (2004a) and Quidelleur et al. (2008) proposed that rapid sea-level rise associated with warmer and wetter climate during the onsets of interglacials caused increased retention of groundwater and pore pressure in volcanic islands, thus favouring their instability. However, these hypotheses rely on incomplete databases of volcano flank collapses that are often inaccurately dated. Hunt et al. (2014) examined 125 volcaniclastic turbidites on the Madeira Abyssal Plain as a record of large (> 5 km³) flank collapses of the Canary Islands. They found no significant statistical correlation between the turbidite occurrence and sea-level change during the last 17 Ma (the record being more complete for the last 7 Ma). Plotting 28 dated flank collapses from 6 archipelagos (Hawaii, Canary Islands, Cape Verde Islands, Reunion Island, Azores, and Society Islands) against the sea-level curve of the last 1 Ma (Fig. 15) confirms no correlation with specific conditions of sea level. Depending on the accuracy of the ages, only 6 to 10 events (20-35 %) might coincide with periods of rapid sea-level rise (> 5 m/ka, as defined by Coussens et al., 2016). At the contrary, 11 events occurred during relative lowstands of sea level (glacials). The age distribution of the flank collapses is not random. They were apparently more frequent during the last 300 ka, with two other clusters at 550-500 ka (Canary Islands) and 830-880 ka (Canary Islands, Hawaii, and Tahiti-Nui). The example of the Canary Islands demonstrates that the large-scale flank instability is closely linked to the history of volcanism (Fig. 16). Large (>10 km³) flank collapses occur all along the construction of the island, both during the shield and rejuvenated stages. Renewed magma supply during the last 4 Ma marks the rapid growth of La Palma, El Hierro and Tenerife (rejuvenated stage), with 11 major flank collapses, 40 volcaniclastic turbidites (10 of them >100 km³), and increasing sedimentation

rate in the Madeira Abyssal Plain (Fig. 16). The period of low magma supply between 6 and 5 Ma coincides with low sedimentary inputs in the abyssal plain, whereas the coeval growth of the eastern shield volcanoes (Fuerteventuera, Lanzarote and Gran Canaria) between 16 and 12 Ma is associated with high sedimentation rates.

Trying to understand the causes of ocean island flank collapses and the source-to-sink transfers of sediments could appear beyond the scope of this paper. However, tsunami deposits represent an indirect sedimentary record of these events and might hold clues for deciphering a part of the enigma. Constraining the source of a tsunami (earthquake, landslide, volcanic eruption, etc.) from its deposits is one of the most challenging issues in tsunami science. Paris et al. (2014) demonstrated that the tsunami sedimentary record can be coupled with eruptive history (e.g. 1883 Krakatau eruption and tsunamis), especially when the tsunami deposits are interbedded with primary or reworked pyroclastic deposits. The Icod flank collapse and tsunamis in Tenerife represent another relevant case-study. Major and trace element analysis of the pumice clasts incorporated in the different subunits of tsunami deposits (Paris et al., 2017) revealed that the retrogressive failure of the northern flank of Tenerife ca. 170 ka ended with the paroxysm of an explosive ignimbrite-forming eruption (El Abrigo).

In theory, bioclasts included in tsunami deposits could be used as a proxy for reconstructing the climatic conditions that prevailed when the tsunami occurred. However, inherited sources of bioclasts (e.g. elevated marine terraces or offshore palaeoreefs eroded by the tsunami) might cover the tracks of other palaeoclimatic proxies. For instance, the interglacial fauna found in the Agaete tsunami conglomerate (Meco et al., 2002) is not concordant with the age of the tsunami source proposed by Perez-Torrado et al. (2006), i.e. the Güímar flank collapse dated to 860-830 ka (Carracedo et al., 2011). The molluscan fauna of the Agaete conglomerate is typical of the Pleistocene interglacials with a sea temperature similar to the present or slightly warmer (Meco et al., 2002). The age interval of the collapse (860-830 ka) is reliable and falls in the glacial MIS 21 (866-814 ka after Lisiecki and Raymo, 2005). A first explanation for this apparent discrepancy is that the tsunami has reworked previous interglacial deposits. Uncertainties on the timing of the collapse(s) and number of tsunamis is another source of complexity (Giachetti et al., 2011; Madeira et al., 2011a). Further works on the palaeontology of tsunami conglomerates will allow us to better understand the processes of incorporation of bioclasts by megatsunami waves.

7. Conclusions and perspectives

Ocean island flank collapses and their tsunami deposits have not revealed all their secrets yet. Considering the lack of correlation between the Middle and Late Pleistocene climate history and the chronology of flank collapses, rapid sea-level rise in the near future would probably not favour flank instability of ocean island volcanoes. Given the uncertainty on the collapse mechanisms, numerical models can yield unrealistic results and any conclusion on hazard assessment is particularly risky. However, their input parameters can be constrained by field-based models, as demonstrated by examples of well-documented examples of flank collapses and tsunami deposits in the Canary and Cape Verde Islands. Further investigations could focus on issues such as: (1) The completion of the catalogue of megatsunamis generated by volcano flank collapses (and not only ocean island volcanoes); (2) The high-energy transfers of sediments from the flanks of the islands to the abyssal plains through detailed studies of the mass-transport deposits and turbidites around ocean islands; (3) The stratigraphy and high-resolution bathymetry of insular shelves (which are often poorly documented); (4) The development of standardised methods for characterising coarse-grained tsunami deposits such as conglomerates (e.g. image analysis of the texture, structure inferred from geophysical surveys); (5) The development of inverse and forward models of tsunami sediment transport that include pebbles and boulders (Sugawara et al., 2014); (6) Testing the robustness of different dating techniques (e.g. luminescence and surface exposure techniques, viscous remanent magnetisation) and refine the chronology of megatsunamis and volcano flank collapse within the framework of the climate changes; (7) Characterising the magmatic system beneath the volcanic edifice prior to its collapse.

(.)

Acknowledgements

Raphaël Paris is particularly grateful to the Editors of Marine Geology, Gert J. De Lange, Michele Rebesco, and Edward Anthony, and to Tim Horscroft for inviting him to lead this review-type article. Ricardo Ramalho acknowledges his IF/01641/2015 FCT Investigator

contract and funding from FCT - UID/GEO/50019/2013 - Instituto Dom Luiz. José Madeira acknowledges his FCT projects PTDC/CTE-GIN/64330/2006 and UID/GEO/50019/2013. Sérgio Ávila acknowledges his IF/00465/2015 research contract funded by Fundação para a Ciência e a Tecnologia (Portugal). This work was partially supported by FEDER funds through the Operational Programme for Competitiveness Factors – COMPETE and by National Funds through FCT - Foundation for Science and Technology under the UID/BIA/50027/2013 and POCI-01-0145-FEDER-006821. The work of Gilles Rixhon, Simon Matthias May and Max Engel is supported by a grant of KölnAlumni e. V. and a Dr. Hohmann Scholarship of the Gesellschaft für Erdkunde zu Köln e. V. This is ClerVolc Laboratory of Excellence contribution number xxx.

References

Abadie, S., Morichon, D., Grilli, S., Glockner, S., 2010. Numerical simulation of waves generated by landslides using a multiple-fluid Navier-Stokes model. Coastal Engineering 57, 779-794.

Abe, K., 1979. Size of great earthquakes of 1957-1974 inferred from tsunami data. Journal of Geophysical Research 84(4), 1561-1568.

Ablay, G.J., Hürlimann, M., 2000. Evolution of the north flank of Tenerife by recurrent giant landslides. Journal of Volcanology and Geothermal Research 103, 135-159.

Amelung, F., Day, S.J., 2002. InSAR observations of the 1995 Fogo, Cape Verde, eruption: implications for the effects of collapse events upon island volcanoes. Geophysical Research Letters 29 (12), 1606.

Ancochea, E., Huertas, M.J., Cantagrel, J.M., Coello, J., Fúster, J.M., Arnaud, N., Ibarolla, E., 1999. Evolution of the Cañadas edifice and its implications for the origin of the Las Cañadas Caldera (Tenerife, Canary Islands). Journal of Volcanology and Geothermal Research 88, 177-199.

Ávila, S.P., Melo, C., Silva, L., Ramalho, R., Quartau, R., Hipólito, A., Cordeiro, R., Rebelo, A.C., Madeira, P., Rovere, A., Hearty, P.J., Henriques, D., Silva, C.M., Martins, A.M.F., Zazo, C., 2015. A review of the MIS 5e highstand deposits from Santa Maria

Island (Azores, NE Atlantic): palaeobiodiversity, palaeoecology and palaeobiogeography. Quaternary Science Reviews 114, 126-148.

Bachèlery, P., Mairine, P., 1990. Evolution volcano-structurale du Piton de la Fournaise depuis 0.53 Ma. In: Lénat J.F. (Ed.), Le volcanisme de la Réunion, monographie. Centre de Recherches en Volcanologie, Clermont-Ferrand, France, 213–242.

Barbano, M.S., Pirrotta, C., Gerardi, F., 2010. Large boulders along the south-eastern Ionian coast of Sicily: storm or tsunami deposits? Marine Geology 275, 140–154.

Berthod, C., Famin, V., Bascou, J., Michon, L., Ildefonse, B., Monié, P., 2016. Evidence of sheared sills related to flank destabilization in a basaltic volcano. Tectonophysics 674, 195-209.

Bonaccorso, A., Calvari, S., Garfì, L., Lodato, L., Patanè, D., 2003. Dynamics of the December 2002 flank failure and tsunami at Stromboli volcano inferred by volcanological and geophysical observations. Geophysical Research Letters 30, 1941.

Boulesteix, T., Hildenbrand, A., Gillot, P.Y., Soler, V., 2012. Eruptive response of oceanic islands to giant landslides: new insights from the geomorphologic evolution of the Teide – Pico Viejo volcanic complex (Tenerife, Canary). Geomorphology 138, 61-73.

Brill, D., Klasen, N., Brückner, H., Jankaew, K., Kelletat, D., Scheffers, A., Scheffers, S., 2012. Local inundation distances and regional tsunami recurrence in the Indian Ocean inferred from luminescence dating of sandy deposits in Thailand. Natural Hazards and Earth System Science 12, 2177–2192.

Brill, D., May, S.M., Shah-Hosseini, M., Rufer, D., Schmidt, C., Engel, M., 2017a. Luminescence dating of cyclone-induced washover fans at Point Lefroy (NW Australia), Quaternary Geochronology, DOI: 10.1016/j.quageo.2017.03.004.

Brown, R.J., Barry, T.L., Branney, M.J., Pringle, M.S., Bryan, S.E., 2003. The Quaternary pyroclastic successions of southeast Tenerife, Canary Islands: explosive eruptions, relative caldera-subsidence, and sector collapse. Geological Magazine 140, 265-288.

Brückner, H., Radtke, U., 1989. Fossile Strände und Korallenbänke auf Oahu, Hawaii. In: Kelletat, D. (Ed.), Neue Ergebnisse der Küstenforschung. Vorträge der Jahrestagung Wilhelmshaven 18. und 19. Mai 1989. Essener Geographische Arbeiten 17, 291–308.

Bryan, S.E., Martí, J., Cas, R.A.F., 1998. Stratigraphy of the Bandas del Sur Formation: an extracaldera record of Quaternary phonolitic explosive eruptions from the Las Cañadas edifice, Tenerife (Canary Islands). Geological Magazine 135, 605-636.

Campbell, J.F., 1984. Rapid subsidence of Kohala volcano and its effect on coral reef growth. Geo-Marine Letters 4, 31-36.

Candy, I., Black, S., Sellwood, B.W., 2005. U-series isochron dating of immature and mature calcretes as a basis for constructing Quaternary landform chronologies for the Sorbas basin, southeast Spain. Quaternary Research 64, 100-111.

Carracedo, J.C., 1996. A simple model for the genesis of large gravitational landslide hazards in the Canary Islands. In: McGuire, Jones, Neuberg (Eds.) Volcano Instability on the Earth and Other Planets. Geological Society Special Publication 110, 125–135.

Carracedo, J.C., Day, S., Guillou, H., Rodríguez Badiola, E., Canas, J.A., Pérez-Torrado, F.J., 1998. Hotspot volcanism close to a passive continental margin: the Canary Islands. Geological Magazine 135 (5), 591-604.

Carracedo, J.C., Day, S., Guillou, H., Pérez-Torrado, F.J., 1999. Giant Quaternary landslides in the evolution of La Palma and El Hierro, Canary Islands. Journal of Volcanology and Geothermal Research 94, 169-190.

Carracedo, J.C., Rodríguez Badiola, E., Guillou, H., Paterne, M., Scaillet, S., Perez-Torrado, F.J., Paris, R., Fra Paleo, U., Hansen, A., 2007. The Teide volcano and the rift-zones of Tenerife, Canary Islands: eruptive and structural history. Geological Society of America Bulletin 119, 1027-1051.

Carracedo, J.C., Guillou, H., Nomade, S., Rodríguez Badiola, E., Perez-Torrado, F.J., Rodríguez Gonzáles, A., Paris, R., Troll, V.R., Wiesmaier, S., Delcamp, A., Fernández Turiel, J.L., 2011. Evolution of ocean island rifts: the northeast rift-zone of Tenerife, Canary Islands. Geological Society of America Bulletin 123, 562-584.

Cayol, V., Catry, T., Michon, L., Chaput, M., Famin, V., Bodart, O., Froger, J.-L., Romagnoli, C., 2014. Sheared sheet intrusions as mechanism for lateral flank displacement on basaltic volcanoes: applications to Réunion Island volcanoes. Journal of Geophysical Research - Solid Earth 119, 7607–7635.

Cisternas, M., Atwater, B.F., Torrejon, F., Sawai, Y., Machuca, G., Lagos, M., Eipert, A., Youlton, C., Salgado, I., Kamataki, T., Shishikura, M., Rajendran, C.P., Malik, J.K., Rizal, Y., Husni, M., 2005. Predecessors of the giant 1960 Chile earthquake. Nature 437, 404–407.

Coello Bravo, J.J., Martín González, M.E., Hernández Gutiérrez L.E., 2014. Tsunami deposits originated by a giant landslide in Tenerife (Canary Islands). Vieraea 42, 79-102.

Cooke, R.J.S., 1981. Eruptive history of the volcano at Ritter Island. Geological Survey of Papua New Guinea Memoir 10, 115-123.

Cornu, M.N., Paris, R., Doucelance, R., Bachélery, P., Guillou, H., 2017. Exploring the links between volcano flank collapse and magma evolution: Fogo oceanic shield volcano, Cape Verde. Geophysical Research Abstracts 19, EGU2017-4875.

Costa, A.C.G., Hildenbrand, A., Marques, F.O., Sibrant, A.L.R., Santos dos Camps, A., 2015. Catastrophic flank collapses and slumping in Pico Island during the last 130 kyr (Pico-Faial ridge, Azores Triple Junction). Journal of Volcanology and Geothermal Research 302, 33-46.

Coussens, M., Wall-Palmer, D., Talling, P.J., Watt, S.F.L., Cassidy, M., Jutzeler, M., Clare, M.A., Hunt, J.E., Manga, M., Gernon, T.M., Palmer, M.R., Hatter, S.J., Boudon, G., Endo, D., Fujinawa, A., Hatfield, R., Hornbach, M.J., Ishizuka, O., Kataoka, K., Le Friant, A., Maeno, F., McCanta, M., Stinton, A.J., 2016. The relationship between eruptive activity, flank collapse, and sea level at volcanic islands: A long-term (>1 Ma) record offshore Montserrat, Lesser Antilles. Geochemistry, Geophysics, Geosystems 17, 2591–2611.

Criado, C., Yanes, A., 2005. Acerca de las paleoformas marinas cuaternarias de Teno Bajo (Tenerife, Islas Canarias). In: Santjaume, E., Mateu, J.F. (Eds.) Geomorfologia litoral y quaternary. Homenatge al Professor Vicenç Roselló I Verger. PUV, Valencia, 113-122.

Crook, K.A.W., Felton, E.A., 2008. Sedimentology of rocky shorelines: 5. The marine samples at +326m from 'Stearns swale' (Lanai, Hawaii) and their paleo-environmental and sedimentary process implications. Sedimentary Geology 206, 33-41.

Dávila Harris, P., Branney, M.J., Storey, M., 2011. Large eruption-triggered ocean-island landslide at Tenerife: onshore record and long-term effects on hazardous pyroclastic dispersal. Geology 39, 951-954.

Day, S.J., Heleno da Silva, S.I.N., Fonseca, J.F.B.D., 1999. A past giant lateral collapse and present-day flank instability of Fogo, Cape Verde Islands. Journal of Volcanology and Geothermal Research 99, 191-218.

Delcamp, A., van Wyk de Vries, B., James, M.R., Lebas, E., 2011. Relationships between volcano gravitational spreading and magma intrusion. Bulletin of Volcanology 74, 743-765.

Denizot, G., 1934. Sur la structure des Iles Canaries, considérée dans ses rapports avec le problème de l'Atlantide. Compte Rendus d'Académie des Sciences 199, 372-373.

Di Risio, M., De Girolamo, P., Beltrami, G.M., 2011. Forecasting landslide generated tsunamis: a review. In: Märner, N.A. (Ed.), The tsunami threat – research and technology. Intech, 26 p.

Driscoll, E.M., Hendry, G.L., Tinkler, K.J., 1965. The geology and geomorphology of Los Ajaches, Lanzarote. Geological Journal, Liverpool, 4, 321-334.

Engel, M., May, S.M., 2012. Bonaire's boulder fields revisited: Evidence for Holocene tsunami impact on the Leeward Antilles. Quaternary Science Reviews 54, 126-141.

Falvard, S., Paris, R., 2017. X-ray tomography of tsunami deposits: towards a new depositional model of tsunami deposits. Sedimentology 64, 453-477.

Feldens, P., Schwarzer, K., Sakuna, D., Szczuciński, W., Sompongchaiyakul, P., 2012. Sediment distribution on the inner continental shelf off Khao Lak (Thailand) after the 2004 Indian Ocean tsunami. Earth, Planets and Space 64, 875–887.

Felton, E.A., 2002. Sedimentology of rocky shorelines: 1. A review of the problem, with analytical methods, and insights gained from the Hulopoe Gravel and the modern rocky shoreline of Lanai, Hawaii. Sedimentary Geology 152, 221-245.

Felton, E.A., Crook, K.A.W., Keating, B.H., Kay, E.A., 2006. Sedimentology of rocky shorelines: 4. Coarse gravel lithofacies, molluscan biofacies, and the stratigraphic and

eustatic records in the type area of the Pleistocene Hulopoe Gravel, Lanai, Hawaii. Sedimentary Geology 184, 1-76.

Fernández-Nieto, E.D., Bouchut, F., Bresch, B., Castro Díaz, M.J., Mangeney, A., 2008. A new Savage-Hutter type model for submarine avalanches and generated tsunami. Journal of Computational Physics 227, 7720-7754.

Ferrer, M., González de Vallejo, L., Seisdedos, J., Coello, J.J., Carlos García, J., Hernández, L.E., Casillas, R., Martín, C., Rodríguez, J.A., Madeira, J., Andrade, C., Freitas, M.C., Lomoschitz, A., Yepes, J., Meco, J., Betancort, J.F., 2013. Güímar and La Orotava mega-landslides (Tenerife) and tsunamis deposits in Canary Islands. In: Margottini, C., Canuti, P., Sassa, K. (Eds.) Landslide Science and Practice, Volume 5, Complex Environment. Springer-Verlag Berlin Heidelberg, 27-33.

Foeken, J.P.T., Day, S.J., Stuart; F.M., 2009. Cosmogenic 3He exposure dating of the Quaternary basalts from Fogo, Cape Verdes: Implications for rift-zone and magmatic reorganisation. Quaternary Geochronology 4 (1), 37-49.

Frenz, M., Wynn, R.B., Georgiopoulou, A., Bender, V.B., Hough, G., Masson, D.G., Talling, P.J., Cronin, B., 2009. Provenance and pathways of late Quaternary turbidites in the deep-water Agadir Basin, northwest African margin. International Journal of Earth Sciences 98, 721-733.

Garcia, M.O., 1996. Turbidites from slope failure on Hawaiian volcanoes. In: McGuire, W.J., Jones, A.P., Neuberg, J. (Eds.) Volcano instability on the Earth and other planets. Geological Society London Special Publication 110, 281-294.

Giachetti, T., Paris, R., Kelfoun, K., (2011). Numerical modelling of the tsunami triggered by the Güìmar debris avalanche, Tenerife (Canary Islands): comparison with field-based data. Marine Geology 284, 189-202.

Goff, J., Terry, P., Chagué-Goff, C., Goto, K., 2014. What is a mega-tsunami? Marine Geology 358, 12–17.

Grigg, R.W., Jones, A.T., 1997. Uplift caused by lithospheric flexure in the Hawaiian archipelago, as revealed by elevated coral deposits. Marine Geology 141, 11-25.

Guillou, H., Carracedo, J.C., Pérez-Torrado, F., Rodriguez-Badiola, E., 1996. K-Ar ages and magnetic stratigraphy of a hotspot-induced, fast grown oceanic island: El Hierro, Canary Islands. Journal of Volcanology and Geothermal Research 73, 141-155.

Hatori, T., 1986. Classification of tsunami magnitude scale. Bull. Earthquake Res. Inst. Univ. Tokyo, 61, 503-515.

Hildenbrand, A., Gillot, P.Y., Leroy, I., 2004. Volcano-tectonic and geochemical evolution of an oceanic intra-plate volcano: Tahitu-Nui (French Polynesia). Earth and Planetary Science Letters 217, 349-365.

Holcomb, R.T., Searle, R.C., 1991. Large landslides from oceanic volcanoes. Marine Geotechnology 10, 19-32.

Huppert, K.L., Royden, L.H., Perron, J.T., 2015. Dominant influence of volcanic loading on vertical motions of the Hawaiian Islands. Earth and Planetary Science Letters 418, 149-171.

Hunt, J.E., Wynn, R.B., Masson, D.G., Talling, J., Teagle, D.A.H., 2011. Sedimentological and geochemical evidence for multi-stage failure of volcanic island landslides: a case-study from Icod landslide on north Tenerife, Canary Islands. Geochemistry, Geophysics, Geosystems 12, Q12007.

Hunt, J.E., Wynn, R.B., Talling, J., Masson, D.G., 2013a. Multistage collapse of eight western Canary Island landslides in the last 1.5 Ma: Sedimentological and geochemical evidence from subunits in submarine flow deposits. Geochemistry, Geophysics, Geosystems 14, 2159-2181.

Hunt, J.E., Wynn, R.B., Talling, P.J., Masson, D.G., 2013b. Turbidite record of frequency and source of large volume (>100 km3) Canary Island landslides in the last 1.5 Ma: Implications for landslide triggers and geohazards, Geochemistry, Geophysics, Geosystems 14, 2100–2123.

Hunt, J.E., Talling, P.J., Clare, M.A., Jarvis, I., Wynn, R.B., 2014. Long-term (17 Ma) turbidite record of the timing and frequency of large flank collapses of the Canary Islands. Geochemistry, Geophysics, Geosystems 15, 3322-3345.

Iida, K., 1963. Magnitude, energy and generation mechanisms of tsunamis and a catalogue of earthquakes associated with tsunamis. Proc. Tsunami Meeting, 10th Pacific Sci. Congress, 1961, IUGG Monograph, 24, 7-18.

Imamura, A., 1942. History of Japanese tsunamis. Kayo-No-Kagaku (Oceanography), 2(2), 74-80 (in Japanese).

Johnson, R.W., 1987. Large-scale volcanic cone collapse; the 1888 slope failure of Ritter volcano. Bulletin of Volcanology 49, 669-679.

Johnson, M.E., Uchman, A., Costa, P.J.M., Ramalho, R.S., Ávila, S.P., 2017. Intense hurricane transport sand onshore: example from the Pliocene Malbusca section on Santa Maria Island (Azores, Portugal). Marine Geology 385, 244-249.

Keating, B.H., McGuire, W.J., 2000. Island edifice failures and associated tsunami hazards. Pure and Applied Geophysics 157, 899-955.

Kelfoun, K., Giachetti, T., Labazuy, P., 2010. Landslide-generated tsunamis at Reunion Island. Journal of Geophysical Research 115, F04012.

Klug, H., 1968. Morphologische Studien auf den Kanarischen Inseln. Beiträge zur Küstenentwicklung und Talbildung auf einem vulkanischen Archipel. Schriften des Geographischen Instituts der Universität Kiel 24(3), 1-184.

Klügel, A., Longpré, M.A., Garcia-Cañada, L., Stix, J., 2015. Deep intrusions, lateral magma transport and related uplift at ocean island volcanoes. Earth and Planetary Science Letters 431, 140-149.

Krastel, S., Schmincke, H.-U., Jacobs, C.L., Richm, R., Le Bas, T.P., Alibé´s, B., 2001. Submarine landslides around the Canary Islands. Journal of Geophysical Research. 106 (B3), 3977– 3997.

Labazuy, P., 1996. Recurrent landsliding events on the submarine flanks of Piton de la Fournaise volcano (Reunion Island). In: McGuire, W.J., Jones, A.P., Neuberg, J. (Eds.), Volcano instability on the Earth and other planets. Geological Society, London, Special Publications 110, 293-306.

Lagmay, A.M.F., van Wyk de Vries, B., Kerle, N., Pyle, D.M., 2000. Volcano instability induced by strike-slip faulting. Bulletin of Volcanology 62, 331-346.

Le Bas, T. P., Masson, D. G., Holtom, R. T., Grevemeyer, I., 2007. Slope failures on the flanks of the southern Cape Verde Islands. In: Lykousis, V., Sakellariou, D., Locat J. (Eds), Submarine Mass Movements and Their Consequences. Springer, Dordrecht, Netherlands, 337-345.

Le Roux, J.P., Gómez, C., Fenner, J., Middleton, H., 2004. Sedimentological processes in a scarp-controlled rocky shoreline to upper continental slope environnement, as revealed by unusual sedimentary features in the Neogene Coquimbo Formation, north-central Chile. Sedimentary Geology 165, 67-92.

Le Roux, J.P., Vargas, G., 2005. Hydraulic behavior of tsunami backflows: insight from their modern and ancient deposits. Environmental Geology 49, 65-75.

Lecointre, G., 1963. Sur les terrains sédimentaires de l'île de Sal, avec remarques sur les îles de Santiago et Maio (Archipel du Cap Vert). Garcia de Orta 11 (2), 275-289.

Lecointre, G., Tinkler, K.J., Richards, G., 1967. The Marine Quaternary of the Canary Islands. Proceedings of the Academy of Natural Sciences of Philadelphia 119, 325-344.

Lipman, P.W., Normark, W.R., Moore, J.G., Wilson, J.B., Gutmacher, C., 1988. The giant submarine Alika debris slide, Mauna Loa, Hawaii. Journal of Geophysical Research 93, 4279-4299.

Lisiecki, L.E., Raymo, M.E., 2005. A Pliocene-Pleistocene stack of 57 globally distributed benthic $\delta^{18}O$ records. Paleooceanography 20, PA1003.

Løvholt, F., Pedersen, G., Gisler, G., 2008. Oceanic propagation of a potential tsunami from the La Palma Island. Journal of Geophysical Research 113, C09026.

Løvholt, F., Pedersen, G, Harbitz, C.B., Glimsdal, S., Kim, J., 2015. On the characteristics of landslide tsunamis. Philosophical Transactions of the Royal Society A 373, 20140376.

Ludwig, K.R., Szabo, B.J., Moore, J.G., Simmons, K.R., 1991. Crustal subsidence rate off Hawaii determined from $^{234}U/^{238}U$ ages of drowned coral reefs. Geology 19, 171-174.

Madeira, J., Ferrer Gijón, M., Gonzalez de Vallejo, L.I., Andrade, C., Freitas, M., Lomoschitz, A., Hoffman, D.L., 2011a. Agaete revisited: new data on the Gran Canaria tsunamiites. Geophysical Research Abstracts 13, EGU2011-2292-2.

Madeira, J., Mata, J., Moreira, M., Hoffman, D.L., 2011b. Deposits of a major Pleistocene tsunami in the Island of Maio (Cape Verde). Geophysical Research Abstracts 13, EGU2011-1995.

Madeira, J., Mata, J., Moreira, M., Ramalho, R.S., 2017. Tsunami deposits in the Island of Maio (Cape Verde): paleocurrent markers and basal erosion features. 5th International Tsunami Field Symposium, Lisbon, 3-7 September 2017.

Manconi, A., Longpré, M.A., Walter, T.R., Troll, V.R., Hansteen, T.H., 2009. The effects of flank collapses on volcano plumbing systems. Geology 37 (12), 1099–1102.

Maramai, A., Graziani, L., Alessio, G., Burrato, P., Colini, L., Cucci, L., Nappi, R., Nardi, A., Vilardo, G., 2005. Near- and far-field survey report of the 30 December 2002 Stromboli Southern Italy tsunami. Marine Geology 215, 93-106.

Martí, J., Mitjavila, J., Araña, V., 1994. Stratigraphy, structure and geochronology of the Las Cañadas caldera, Tenerife, Canary Islands. Geological Magazine 131, 715-727.

Massari, F., D'Alessandro, A., Davaud, E., 2009. A coquinoid tsunamite from the Pliocene of Salento (SE Italy). Sedimentary Geology 221, 7-18.

Masson, D.G., Watts, A.B., Gee, M.R.J., Urgeles, R., Mitchell, N.C., Le Bas, T.P. Canals, M., 2002. Slope failures on the flanks of the western Canary islands. Earth Science Reviews 57, 1–35.

Masson, D.G., Le Bas, T.P., Grevemeyer, I., Weinrebe, W., 2008. Flank collapse and large-scale landsliding in the Cape Verde Islands, off West Africa. Geochemistry, Geophysics, Geosystems 9, Q07015.

Matsutomi, H., Okamoto, K., Harada, K., 2011. Inundation flow velocity of tsunami inland and its practical use. Coastal Engineering Proceedings 32, currents 5.

McMurtry, G.M., Herrero-Bervera, E., Cremer, M.D., Smith, J.R., Resig, J., Sherman, C., Torresan, M.E., 1999. Stratigraphic constraints on the timing and emplacement of the Alika 2 giant Hawaiian submarine landslide. Journal of Volcanology and Geothermal Research 94, 35-58.

McMurtry, G. M., Watts, P., Fryer, G., Smith, J.R., Imamura, F., 2004a. Giant landslides, mega-tsunamis, and paleo-sea level in the Hawaiian Islands. Marine Geology 203**,** 219-233.

McMurtry, G.M., Fryer, G.J., Tappin, D.R., Wilkinson, I.P., Williams, M., Fietzke, J., Garbe-Schoenberg, D., Watts, P., 2004b. Megatsunami deposits on Kohala volcano, Hawaii, from flank, collapse of Mauna Loa. Geology 32 (9), 741-744.

McMurtry, G.M., Tappin, D.R., Sedwick, P.N., Wilkinson, I., Fietzke, J., Sellwood, B., 2007. Elevated marine deposits in Bermuda record a late Quaternary megatsunami. Sedimentary Geology 200, 155–165.

Meco, J., 1989. Islas Canarias. In: Pérez-González, A., Cabra Gil, P., Martín Serrano, A. (Coordinators), Mapa del Cuaternario de España a escala 1:100000. Instituto Tecnológico y Geominero de España.

Meco, J. (Ed.), 2008. Historia geológica del clima en Canarias. Monografia, Universidad Las Palmas de Gran Canaria, Spain, 296 p.

Meco, J., Stearns, C.E., 1981. Emergent littoral deposits in the Eastern Canary Islands. Quaternary Research 15, 199-208.

Meco, J., Guillou, H., Carracedo, J.C., Lomoschitz, A., García Ramos, A.J., Rodríguez-Yáñez, J.J., 2002. The maximum warmings of the Pleistocene world climate recorded in the Canary Islands. Palaeogeogr. Palaeoclimatol. Palaeoecol. 185 (1-2), 197-210.

Meco, J., Scailet, S., Guillou, H., Lomoschitz, A., Carracedo, J.C., Ballester, J., Betancort, J.F., Cilleros, A., 2007. Evidence for long-term uplift on the Canary Islands from emergent Mio-Pliocene littoral deposits. Global and Planetary Change 57, 222-234.

Menard, H.W., 1983. Insular erosion, isostasy and subsidence. Science 220, 913-918.

Menard, H.W., 1986. Islands. Scientific American Library, New York, 231 p.

Menendez, I., Silva, P.G., Martín-Betancor, M., Perez-Torrado F.J., Guillou, H., Scaillet, S., 2008. Fluvial dissection, isostatic uplift, and geomorphological evolution of volcanic islands (Gran Canaria, Canary Islands, Spain). Geomorphology 102, 189-203.

Merle, O., Mairine, P., Michon, L., Bachèlery, P., Smietana, M., 2010. Calderas, landslides and paleo-canyons on Piton de la Fournaise volcano (La Réunion Island, Indian Ocean). Journal of Volcanology and Geothermal Research 189, 131-142.

Miller, D.J., 1960. Giant waves in Lituya Bay, Alaska. Geological Survey Professional Paper 354-C, U.S. Government Printing Office, Washington D.C.

Mitchell, N.C., 1998. Characterising the irregular coastlines of volcanic ocean islands. Geomorphology 23, 1-14.

Mitchell, N.C., 2003. Susceptibility of mid-ocean ridge volcanic islands and seamounts to large-scale landsliding. Journal of Geophysical Research 108, 2397.

Montaggioni, L., 1978. Recherches géologiques sur les complexes récifaux de l'archipel des Mascareignes (Océan Indien Occidental). Thèse d'Etat, Université d'Aix-Marseille, France.

Moore, A.L., 2000. Landward fining in onshore gravel as evidence for a late Pleistocene tsunami on Molokai, Hawaii. Geology 28 (3), 247-250.

Moore G.W., Moore J.G., 1988. Large-scale bedforms in boulder gravel produced by giant waves in Hawaii. Geological Society of America Special Paper 229, 101-110.

Moore, J.G., 1971. Relationship between subsidence and volcanic load, Hawaii. Bulletin Volcanologique 34, 562-576.

Moore, J.G., 1987. Subsidence of the Hawaiian Ridge. In: Decker, R.W., Wright, T.L., Stauffer, P.H. (Eds.), U.S. Geological Survey Professional Paper 1350, 85-100.

Moore, J.G., Fornari, D.J., 1984. Drowned reefs as indicators of the rate of subsidence of the island of Hawaii. Journal of Geology 92, 753-759.

Moore J.G., Moore G.W., 1984. Deposit from a giant wave on the island of Lanai, Hawaii. Science 226, 1312-1315.

Moore, J.G., Campbell, J.F., 1987. Age of tilted reefs, Hawaii. Journal of Geophysical Research 92, 2641-2646.

Moore, J.G., Clague, D.A., Holcomb, R.T., Lipman, P.W., Normark, W.R., Torresan, M.E., 1989. Prodigious submarine landslides on the Hawaiian Ridge. Journal of Geophysical Research 94, 17465–17484.

Moore, J.G., Bryan, W.B., Ludwig, K.R., 1994. Chaotic deposition by a giant wave, Molokai, Hawaii. Geological Society of America Bulletin 106, 962-967.

Moore, J.G., Ingram, B.L., Ludwig, K.R., Clague, D.A., 1996. Coral ages and island subsidence, Hilo drill hole. Journal of Geophysical Research 101 B5, 11599-11605.

Nandasena, N.A.K., Paris, R., Tanaka, N., 2011. Reassessment of hydrodynamic equations to initiate boulder transport by high energy events (storms, tsunamis). Marine Geology 281, 70-84.

Navarrete, R., Liesa, C.L., Castanera, D., Soria, A.R., Rodríguez-López, J.P., Canudo, J., 2014. A thick Tethyan multi-bed tsunami deposit preserving a dinosaur megatracksite within a coastal lagoon (Barremian, eastern Spain)- Sedimentary Geology 313, 105–127.

Normark, W.R, Moore, J.G., Torresan, M.E., 1993. Giant volcano−related landslides and the development of the Hawaiian Islands. In: Schwab, W.C., Lee, H. J., Twichell, D.C. (Eds.), US Geological Survey Bulletin 2002, 184–196.

Oehler, J.-F., Labazuy, P., Lénat, J.F., 2004. Recurrence of major flank landslides during the last 2−Ma−history of Réunion Island. Bulletin of Volcanology 66, 585–598.

Olson, S.L., Hearty, P.J., 2009. A sustained +21 m sea-level highstand during MIS 11 (400 ka): direct fossil and sedimentary evidence from Bermuda. Quaternary Science Reviews 28, 271–285.

Paris, R., 2002. Rythmes de construction et de destruction des édifices volcaniques de point chaud : l'exemple des Iles Canaries (Espagne). PhD Thesis, Université Paris 1 Panthéon-Sorbonne & Universidad de Las Palmas de Gran Canaria, 376 pp.

Paris, R., Perez-Torrado, F.J., Cabrera, M.C., Schneider, J.L., Wassmer, P., Carracedo, J.C., 2004. Tsunami-induced conglomerates and debris flow deposits on the western coast of Gran Canaria (Canary Islands). Acta Vulcanologica 16(1), 133-136.

Paris, R., Perez-Torrado, F.J., Carracedo, J.C., 2005. Massive flank failures and tsunamis in the Canary Islands: past, present, future. Zeitschrift für Geomorphologie Suppl. Band 140, 37-54.

Paris, R., Fournier, J., Poizot, E., Etienne, S., Morin, J., Lavigne, F., Wassmer, P., 2010. Boulder and fine sediment transport and deposition by the 2004 tsunami in Lhok Nga (western Banda Aceh, Sumatra, Indonesia): a coupled offshore – onshore model. Marine Geology 268, 43-54.

Paris, R., Giachetti, T., Chevalier, J., Guillou, H., Frank, N., 2011. Tsunami deposits in Santiago Island (Cape Verde archipelago) as possible evidence of a massive flank failure of Fogo volcano. Sedimentary Geology 239, 129-145.

Paris, R., Kelfoun, K., Giachetti, T., 2013. Marine conglomerate and reef megaclasts at Mauritius Island (Indian Ocean): evidences of a tsunami generated by a flank collapse of Piton de la Fournaise volcano, Réunion Island? Science of Tsunami Hazards 32, 281-291.

Paris, R., Wassmer, P., Lavigne, F., Belousov, A., Belousova, M., Iskandarsyah, Y., Benbakkar, M., Ontowirjo, B., Mazzoni, N., 2014. Coupling eruption and tsunami records: the Krakatau 1883 case-study, Indonesia. Bulletin of Volcanology 76, 814.

Paris, R., Coello Bravo, J.J., Martín González, M.E., Kelfoun, K., Nauret, F., 2017. Explosive eruption, flank collapse and mega-tsunami at Tenerife ca. 170 ky ago. Nature Communications xxx.

Perez-Torrado, F.J., Paris, R., Cabrera, M.C., Carracedo, J.C., Schneider, J.L., Wassmer, P., Guillou, H., Gimeno, D., 2002. Depósitos de tsunami en el valle de Agaete, Gran Canaria (Islas Canarias). Geogaceta 32 (2002), 75-78.

Perez-Torrado, F.J., Paris, R., Cabrera, M.C., Schneider, J.L., Wassmer, P., Carracedo, J.C., Rodriguez Santana, A., Santana, F., 2006. The Agaete tsunami deposits (Gran Canaria): evidence of tsunamis related to flank collapses in the Canary Islands. Marine Geology 227 (1-2), 137-149.

Quidelleur, X., Hildenbrand, A., Samper, A., 2008. Causal link between Quaternary paleoclimatic changes and volcanic islands evolution. Geophysical Research Letters 35, L02303.

Ramalho, R.S., Helffrich, G., Cosca, M., Vance, D., Hoffman, D., Schmidt, D.N., 2010a. Vertical movements of ocean island volcanoes: Insights from a stationary plate environment. Marine Geology 275, 84-95.

Ramalho, R.S., Helffrich, G., Cosca, M., Vance, D., Hoffman, D., Schmidt, D.N., 2010b. Episodic swell growth inferred from variable uplift of the Cape Verde hot spot islands. Nature Geoscience 3, 774–777.

Ramalho, R.S., Winclker, G., Madeira, J., Helffrich, G.R., Hipólito, A.R., Quartau, R., Adena, K., Schaefer, J.M., 2015. Hazard potential of volcanic flank collapses raised by new megatsunami evidence. Science Advances 1 (2015), e1500456.

Ramalho, R.S., Helffrich, G., Madeira, J., Cosca, M., Thomas, C., Quartau, R., Hipólito, A., Rovere, A., Ávila, S. 2017. Emergence and evolution of Santa Maria Island (Azores) – The conundrum of uplifted islands revisited. Geological Society of America Bulletin 129 (3-4), 372–391.

Rixhon, G., May, S.M., Engel, M., Mechernich, S., Schroeder-Ritzrau, A., Frank, N., Fohlmeister, J., Boulvain, F., Dunai, T., Brückner, H., 2017a. Multiple dating approach (^{14}C, $^{230}Th/U$ and ^{36}Cl) of tsunami-transported reef-top boulders on Bonaire (Leeward Antilles) – current research and future challenges. Marine Geology,DOI: 10.1016/j.margeo.2017.03.007.

Rixhon, G., Briant, R.M., Cordier, S., Duval, M., Jones, A., Scholz, D. 2017b. Revealing the pace of river landscape evolution during the Quaternary: recent developments in numerical dating methods. Quaternary Science Reviews 1-23.

Roberts, R. G., Jacobs, Z., Li, B., Jankowski, N. R., Cunningham, A. C., Rosenfeld, A. B., 2015. Optical dating in archaeology: thirty years in retrospect and grand challenges for the future. Journal of Archaeological Science 56, 41-60.

Rubin, K.H., Fletcher III, C.H., Sherman, C., 2000. Fossiliferous Lanai'I deposits formed by multiple events rather than a single giant tsunami. Nature 408, 675-681.

Sanderson, D.C.W., Murphy, S., 2010. Using simple portable OSL measurements and laboratory characterization to help understand complex and heterogeneous sediment sequences for luminescence dating. Quaternary Geochronology 5, 299-305.

Satake, K., Kato, Y., 2001. The 1741 Oshima-Oshima eruption: extent and volume of submarine debris avalanche. Geophysical Research Letters 28, 427-430.

Schellmann, G., Radtke, U., Brückner, H., 2011. Electron spin resonance dating (ESR). In: Hopley, D. (Ed.), Encyclopedia of Modern Coral Reefs - Structure, Form and Process. Springer, Dordrecht, pp. 368–372.

Serralheiro, A., 1976. A geologia da ilha de Santiago (Cabo Verde). Boletim do Museu e Laboratório Mineralógico e Geológico da Faculdade de Ciências de Lisboa 14 (9), 157-372.

Shiki, T., Yamazaki, T., 1996. Tsunami-induced conglomerates in Miocene upper bathyal deposits, Chita Peninsula, central Japan. Sedimentary Geology 104, 175-188.

Sibrant, A.L.R., Marques, F.O., Hildenbrand, A., 2014. Construction and destruction of a volcanic island developed inside an ocean rift: Graciosa, Terceira Rift, Azores. Journal of Volcanology and Geothermal Research 284, 32-45.

Siddall, M., Chappell, J., Potter, E.-K., 2007. Eustatic sea level during past interglacials. Developments in Quaternary Sciences 7, 75-92.

Siebert, L., 1984. Large volcanic debris avalanches: characteristics of source areas, deposits, and associated eruptions. Journal of Volcanology and Geothermal Research 22, 163-197.

Smith, J.R., Wessel, P., 2000. Isostatic consequences of giant landslides on the Hawaiian Ridge. Pure and Applied Geophysics 157, 1097-1114.

Smith, J.R., Satake, K., Morgan, J.K., Lipman, P.W., 2002. Submarine landslides and volcanic features on Kohala and Mauna Kea volcanoes and the Hana Ridge, Hawaii. In: Takahashi, E. et al. (Eds.), Hawaiian volcanoes: deep underwater perspectives. American Geophysical Union Geophysical Monograph 128, 11-28.

Sohbati, R., Murray, A.S., Buylaert, J.-P., Almeida, N.A.C., Cunha, P.P., 2012a. Optically stimulated 678 luminescence (OSL) dating of quartzite cobbles from the Tapada do Montinho archaeological site 679 (east-central Portugal). Boreas, 41, 452-462.

Sohbati, R., Murray, A.S., Chapot, M.S., Jain, M., Pederson, J., 2012b. Optically stimulated luminescence (OSL) as a chronometer for surface exposure dating. J. Geophys. Res. B Solid Earth, 117(9), B09202.

Soloviev, S.L., 1972. Recurrence of earthquakes and tsunamis in the Pacific Ocean. In: Volny Tsunami, Trudy Sakhnii, 29, 7-47 (in Russian).

Stearns, H.T., 1936. H.T. Stearns Field Notebook, vol. 17-2. U.S. Geological Survey Field Office Library, Honolulu, Hawaii, 104-131.

Stearns, H.T., 1938. Ancient shorelines on the islands of Lanai, Hawaii. Geological Society of America Bulletin 49, 615-628.

Stearns, H.T., 1978. Quaternary shorelines in the Hawaiian Islands. Bernice P. Bishop Museum Bulletin 237, 57.

Stearns, H.T., McDonald, G.A., 1946. Geology and groundwater ressources of the Island of Hawaii. Hawaii Division of Hydrography Bulletin 9, 363 p.

Sugawara, D., Goto, K., Jaffe, B.E., 2014. Numerical models of tsunami sediment transport - current understanding and future directions. Marine Geology 352, 295-320.

Suzuki, A., Yokoyama, Y., Kan, H., Minoshima, K., Matsuzaki, H., Hamanaka, N., Kawahata, H., Identification of 1771 Meiwa Tsunami deposits using a combination of radiocarbon dating and oxygen isotope microprofiling of emerged massive Porites boulders. Quaternary Geochronology 3, 226-234.

Synolakis, C.E., Liu, P., Carrier, G., Yeh, H., 1997. Tsunamigenic sea-floor deformations. Science 278, 598-600.

Tanner, L.H., Calvari, S., 2004. Unusual sedimentary deposits on the SE side of Stromboli volcano, Italy: products of a tsunami caused by the ca. 5000 BP Sciarra del Fuoco collapse? Journal of Volcanology and Geothermal Research 137, 329-340.

Van Wyk de Vries, B., Francis, P.W., 1997. Catastrophic collapses at stratovolcanoes induced by gradual volcano spreading. Nature 387, 387-390.

Walter, T.R., Troll, V.R., 2003. Experiments on rift zone formation in unstable volcanic edifices: Journal of Volcanology and Geothermal Research 127, 107–120.

Walter, T.R., Troll, V.R., Cailleau, B., Belousov, A., Schmincke, H.-U., Amelung, F., and Van Den Bogaard, P., 2005. Rift zone reorganization through flank instability in ocean island volcanoes: An example from Tenerife, Canary Islands. Bulletin of Volcanology 67, 281–291.

Ward, S. N., Day, S. 2001. Cumbre Vieja Volcano—Potential collapse and tsunami at La Palma, Canary Islands. Geophysical Research Letters 28, 3397–3400.

Ward, S.N., Day, S., 2003. Ritter Island Volcano-lateral collapse and the tsunami of 1888. Geophysical Journal International 154, 891-902.

Watts, A.B., ten Brink, U.S., 1989. Crustal structure, flexure, and subsidence history of the Hawaiian Islands. Journal of Geophysical Research 94, 10473-10500.

Watts, A.B. and Masson, D.G., 1995. A giant landslide on the north flank of Tenerife, Canary Islands. Journal of Geophysical Research 100, 24,487-24,498 (1995).

Watts, A.B. and Masson, D.G., 2001. New sonar evidence for recent catastrophic collapses of the north flank of Tenerife, Canary Islands. Bulletin of Volcanology 63, 8-19.

Weaver, P.P.E., Jarvis, I., Lebreiro, S.M., Alibes, B., Baraza, J., Howe, R., Rothwell, R.G., 1998. The Neogene turbidite sequence of the Madeira Abyssal Plain-basin filling and diagenesis in the deep ocean. Proceedings of the Ocean Drilling Program 157, 619-634.

Webster, J.M., Clague, D.A., Braga, J.C., Spalding, H., Renema, W., Kelley, C., Applegate, B., Smith, J.R., Paull, C.K., Moore, J.G., Potts, D., 2006. Drowned coralline algal dominated deposits off Lanai, Hawaii ; carbonate accretion and vertical tectonics over the last 30 ka. Marine Geology 225, 223-246.

Webster, J.M., Clague, D.A., Braga, J.C., 2007. Support for the giant wave hypothesis : evidence from submerged terraces off Lanai, Hawaii. International Journal of Earth Sciences 96, 517-524.

Webster, J.M., Clague, D.A., Faichney, I.D.E., Fullagar, P.D., Hein, J.R., Moore, J.G., Paull, C.K., 2010. Early Pleistocene origin of reefs around Lanai, Hawaii. Earth and Planetary Science Letters 290, 331-339.

Wessel, P., 1993. A reexamination of the flexural deformation beneath the Hawaiian Islands. Journal of Geophysical Research 87, 12177-12190.

Wynn, R.B., Weaver, P.E., Stow, D.A.V., Masson, D.G., 2002. Turbidite depositional architecture across three interconnected deep-water basins on the northwest African margin. Sedimentology 49, 669-695.

Yavari-Ramshe S., Ataie-Ashtiani B., 2016. Numerical modeling of subaerial and submarine landslide-generated tsunami waves - recent advances and future challenges. Landslides 2016 (13), 1325-1368.

Zazo, C., Goy, J.L., Hillaire-Marcel, C., Gillot, P.Y., Soler, V., González, J.A., Dabrio, C.J., Ghaleb, B., 2002. Raised marine sequences of Lanzarote and Fuerteventura revisited – a reappraisal of relative sea-level changes and vertical movements in the eastern Canary Islands during the Quaternary. Quaternary Science Reviews 21, 2019-2046.

Zazo, C., Goy, J.L., Hillaire-Marcel, C., González Delgado, J.A., Soler, V., Ghaleb, B., Dabrio, C.J., 2003. Registro de los cambios del nivel del mar durante el Cuaternario en las Islas Canarias Occidentales (Tenerife y La Palma). Estudios Geologicos 59, 133-144.

Zhao, J.-x., Collins, L., 2011. Uranium Series Dating. In: Hopley, D. (Ed.), Encyclopedia of Modern Coral Reefs ‐ Structure, Form and Process. Springer, Dordrecht, pp. 1128–1132.

Figure captions

Fig. 1 – Evidence of megatsunami generated by volcano flank instability in the Hawaiian Islands. Large flank collapse s and their submarine deposits (dotted lines), slumping due to gravitational spreading of the volcanic edifice (slump fronts in bold lines) and tsunami conglomerates (yellow dots). Shaded relief from SOEST (data available at http://www.soest.hawaii.edu/HMRG/multibeam/).

Fig. 2 – Conglomerates on the western coast of Gran Canaria (Agaete Valley, Canary Islands) as an evidence of megatsunami generated by the Güímar massive flank collapse (eastern coast of Tenerife). The collapse scar has a reconstructed volume of 47 km³ (Paris et al., 2005) and is dated to 860-830 ka (Carracedo et al., 2011). The conglomerate mantles the topography at elevations ranging from 41 to 188 m a.p.s.l. (Perez-Torrado et al., 2006).

Fig. 3 – Longitudinal profile of the southern slope of the Agaete valley (western coast of Gran Canaria). The tsunami conglomerates display two subunits: a lower coarse subunit fining landward with clast imbrication oriented landward (eastward), and a finer upper subunit with seaward clast imbrication (westward). Modified from Perez-Torrado et al. (2006).

Fig. 4 – Sedimentary sections of the Agaete tsunami conglomerate (Gran Canaria) showing (A) a downward-injected clastic dyke of the tsunami conglomerate in the substratum (colluvial deposits), and (B) the succession of two distinct tsunami units separated by palaeosols.

Fig. 5 – Spatial distribution (with elevation in meters) of tsunami deposits on the northwestern coast of Tenerife (Canary Islands). Two successive tsunamis were generated ~170 ka ago by a retrogressive failure of the northern flank of the island (Icod collapse) associated with a major explosive eruption (El Abrigo). Modified from Paris et al. (2017).

Fig. 6 – Basaltic boulders imbedded in a coarse sand-to-pebble matrix on the south-western coast of Lanzarote (Canary Islands). Meco (2008) interpreted this deposit as an evidence of tsunami, based on the unusual composition of the molluscan fauna.

Fig. 7 – Megatsunami evidence on the Tarrafal peninsula, northern Santiago (Cape Verde Islands). A: Location map of tsunami conglomerates and megaclasts (modified from Ramalho et al., 2015); B: Megaclast quarried from a scarp (presently at 160-190 m a.p.s.l.) and transported upwards by the tsunami at higher elevation (here at xxx m a.p.s.l.). C: Tsunami conglomerate exposed along the cliff north of Tarrafal Beach.Fig. 8 – Relevant features of the Tarrafal tsunami conglomerate (Cape Verde Islands). A: The coarse matrix is locally enriched in marine bioclasts (note the rhodolites and bivalve shells); B: Coral encrustation attesting for the submarine origin of a boulder; C: scour-and-fill features at the contact between the tsunami conglomerate and the underlying substratum (palaeosol); D: rip-up clasts of volcanic tuff (the substratum) at the base of the tsunami conglomerate.

Fig. 9 - Electrical Resistivity Tomography (ERT) profile showing the upward extension and thickness variation of the tsunami conglomerate below colluvial deposits near Tarrafal (Cape Verde Islands). Additional information on the technique, device and parameters used.

Fig. 10 – Examples of numerical simulations of tsunami inundation at Santiago Island (Cape Verde) following a massive flank collapse of Fogo Island (Monte Amarelo collapse). White dots indicate the tsunami conglomerates and megaclasts on the Tarrafal peninsula. Two types of landslide rheology and two types of scenario are considered: frictional rheology (Mohr-Coulomb type), or plastic rheology (constant retarding stress), applied to a massive or multistage (retrogressive) collapse. See Paris et al. (2011) for more details on the numerical model.

Fig. 11 – Age of the Tarrafal tsunami and Monte Amarelo flank collapse (Cape Verde Islands) inferred from ^{3}He exposure ages of both pre-collapse and post-collapse lavaflows in Fogo Island (Foeken et al., 2009), ^{230Th}/U ages of corals in the tsunami conglomerate (Paris et al., 2011; ref for new age 110 ka Koeln), and ^{3}He exposure ages of tsunami megaclasts in Tarrafal, Santiago Island (Ramalho et al., 2015). Eustatic sea-level curve from Sidall et al. (2007).

Fig. 12 – Tsunami conglomerate near Beau Champ, southern coast of Mauritius Island). The tsunami was most probably generated by a flank collapse of Piton de la Fournaise volcano (Reunion Island) ca. 4.4 ka. Modified from Paris et al. (2013).

Fig. 13 – Imbricated boulders and pebbles overtopping a palaeodune on the south-western coast of Reunion Island.

Fig. 14 – Example of traction carpet at the base of a tsunami conglomerate (Teno tsunami, Tenerife, Canary Islands, cf. Paris et al., 2017). The fine-grained traction carpet is irregularly preserved along the wavy contact between the conglomerate and the underlying lapilli deposit and palaeosol. Note the presence of the rip-up clasts of palaeosol.

Fig. 15 – Age of large (>10 km^3) flank collapses of ocean island volcanoes, and sea level history over the last 1 Ma. Sea level curve after Miller et al. (2005). Ages of the volcano flank collapses after Bachèlery and Mairine (1990), Carracedo et al. (1999, 2007, 2011), Costa et al. (2015), Foeken et al. (2009), Hildenbrand et al. (2004), Hunt et al. (2013b, 2014), Krastel et al. (2001), Oehler et al. (2004), McMurtry et al. (2004a), Masson et al. (2002, 2008), Merle et al. (2010), Paris et al. (2011, 2017), Ramalho et al. (2015), and Sibrant et al. (2014).

Fig. 16 – Volcanic stages and magma supply rates in the Canary Islands (modified after Paris, 2002), sedimentation rates in the Madeira Abyssal Plain (Weaver et al., 1998), and decompacted volumes of volcaniclastic turbidites in the Madeira Abyssal Plain (Hunt et al., 2014).

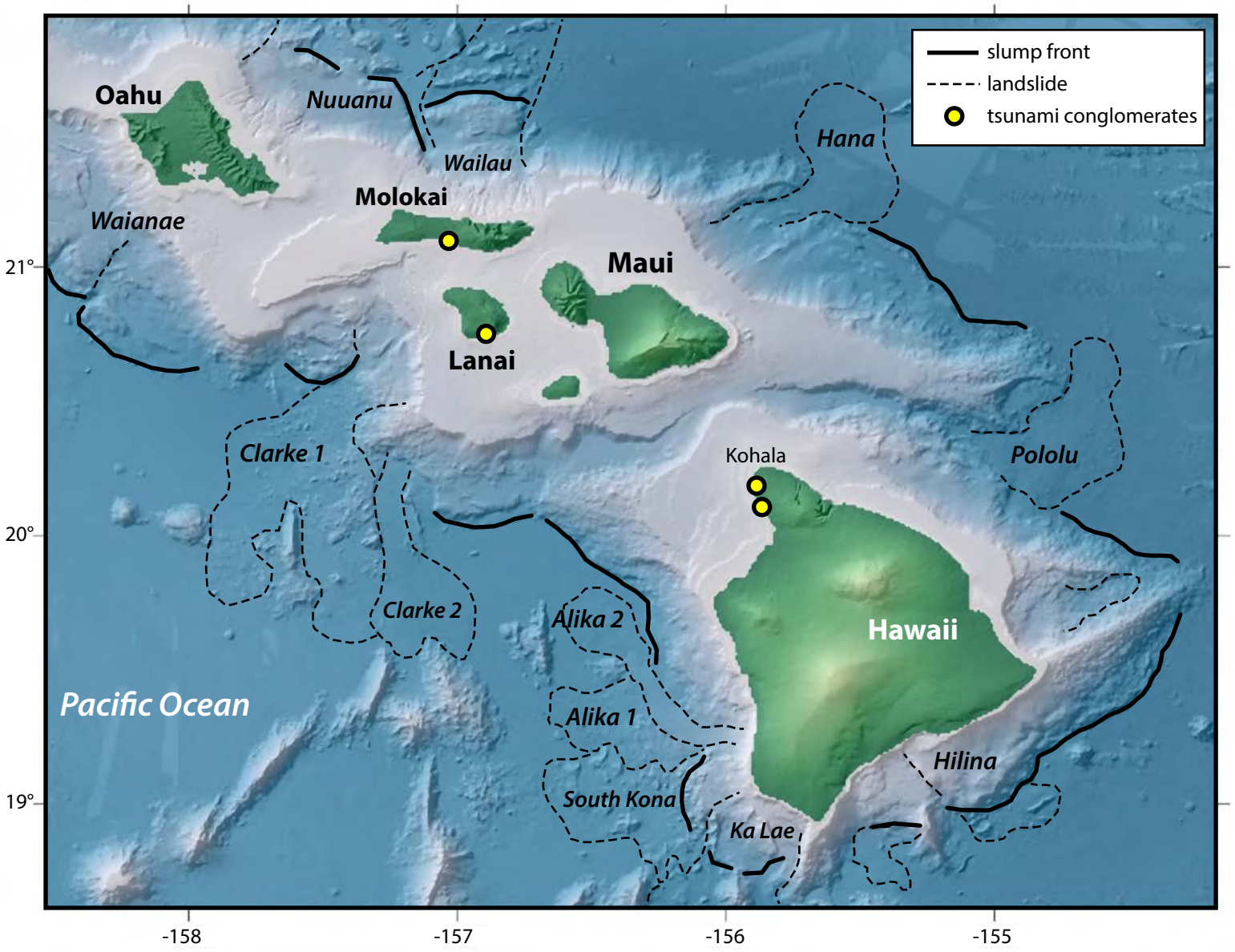
slump front
landslide
tsunami conglomerates
Oahu
Nuuanu
Wailau
Molokai
Waianae
Hana
Maui
Lanai
Clarke 1
Kohala
Pololu
Clarke 2
Alika 2
Hawaii
Pacific Ocean
Alika 1
Hilina
South Kona
Ka Lae
21°
20°
19°
-158
-157
-156
-155

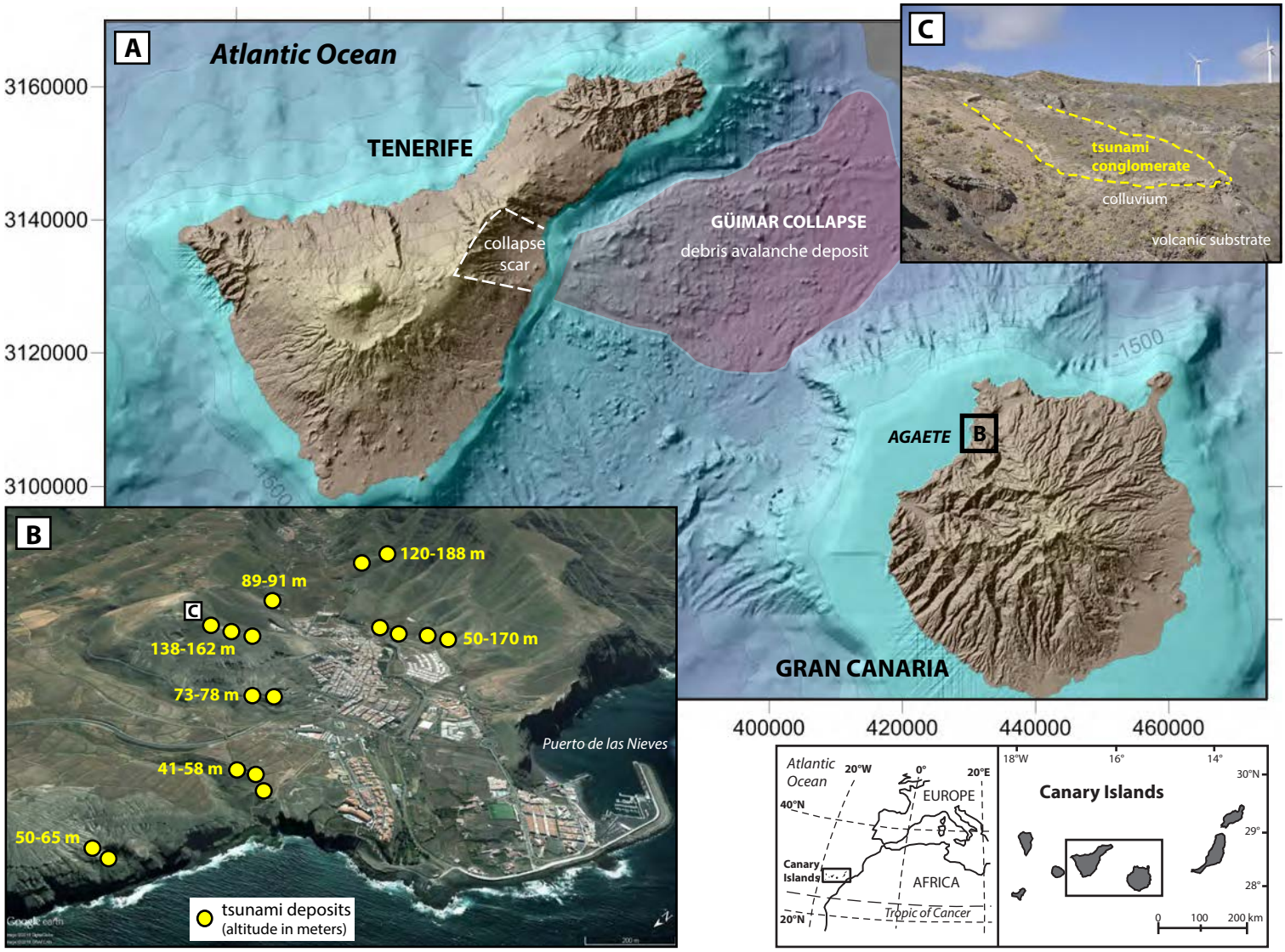
A
Atlantic Ocean
TENERIFE
collapse scar
GÜIMAR COLLAPSE
debris avalanche deposit
AGAETE
B
GRAN CANARIA
-1500
3160000
3140000
3120000
3100000
400000
420000
440000
460000
C
tsunami conglomerate
colluvium
volcanic substrate
B
120-188 m
89-91 m
C
138-162 m
50-170 m
73-78 m
41-58 m
50-65 m
Puerto de las Nieves
tsunami deposits
(altitude in meters)
Atlantic Ocean
20°W
0°
20°E
40°N
EUROPE
Canary Islands
AFRICA
Tropic of Cancer
20°N
18°W
16°
14°
30°N
29°
28°
Canary Islands
0
100
200 km

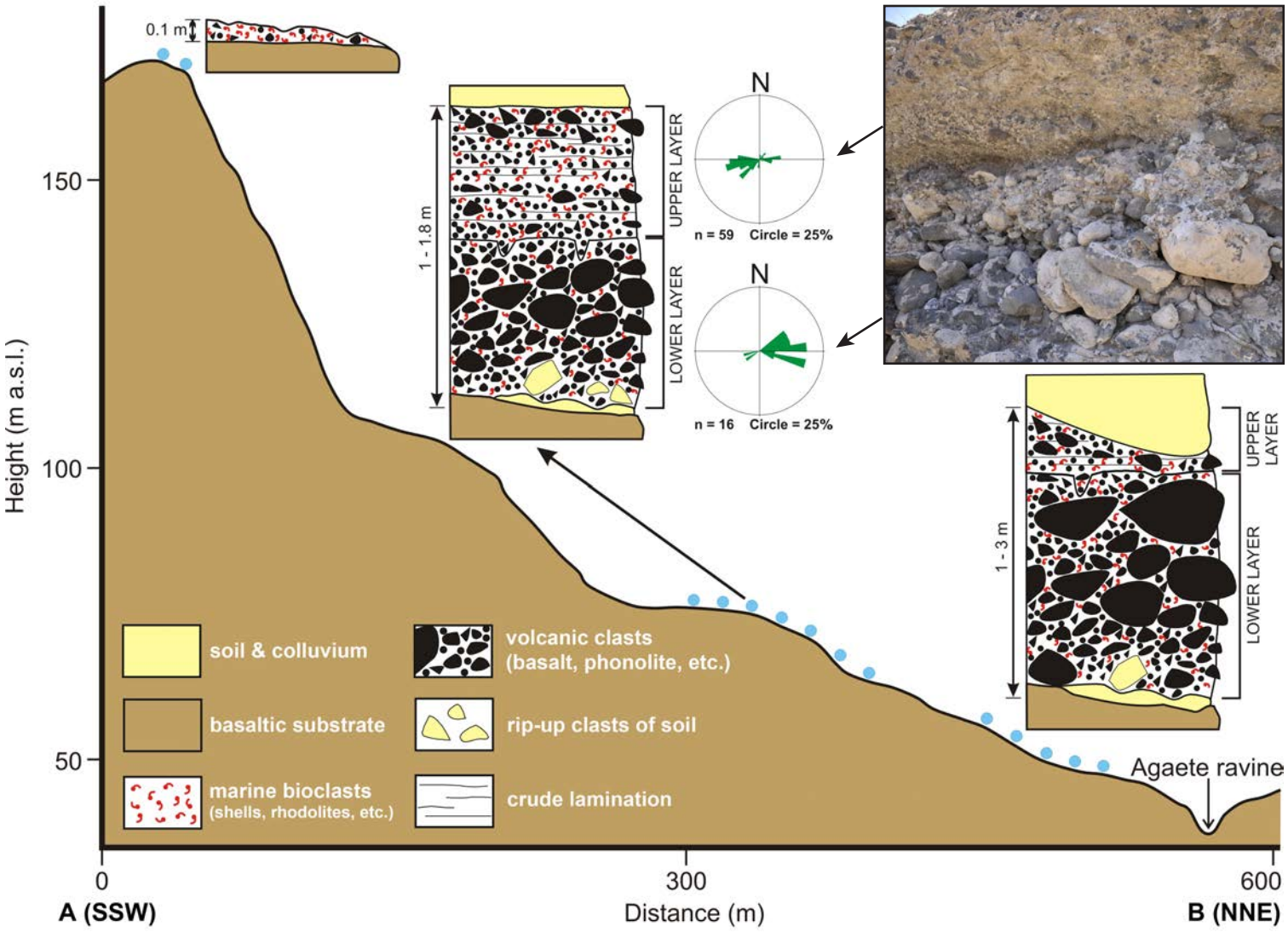
0.1 m
150
100
50
Height (m a.s.l.)
1 - 1.8 m
UPPER LAYER
LOWER LAYER
N
n = 59 Circle = 25%
N
n = 16 Circle = 25%
1 - 3 m
UPPER LAYER
LOWER LAYER
soil & colluvium
basaltic substrate
marine bioclasts
(shells, rhodolites, etc.)
volcanic clasts
(basalt, phonolite, etc.)
rip-up clasts of soil
crude lamination
Agaete ravine
0
300
600
A (SSW)
Distance (m)
B (NNE)

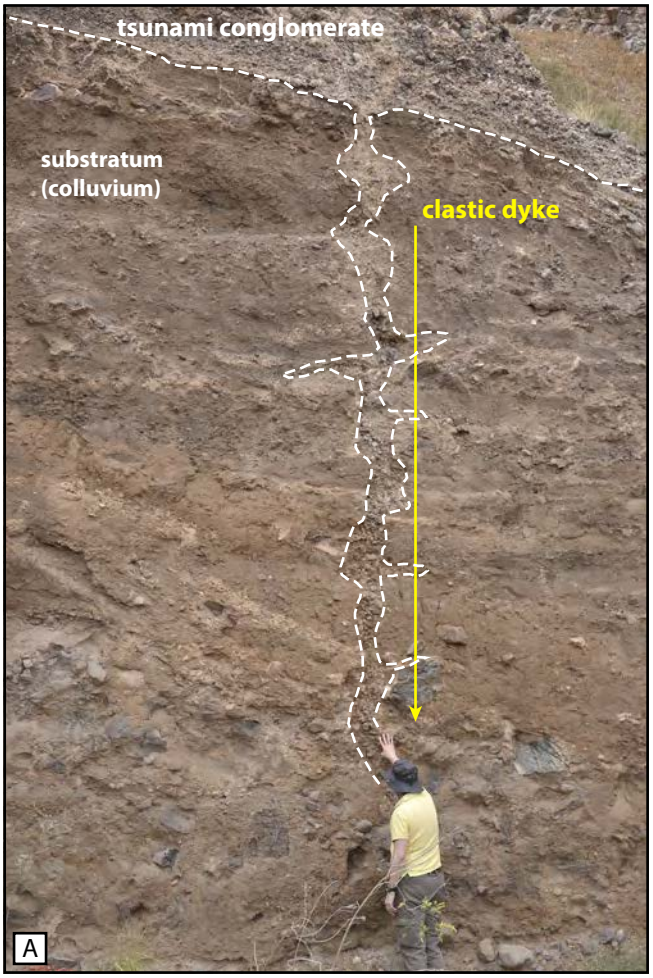
tsunami conglomerate
substratum
(colluvium)
clastic dyke
A

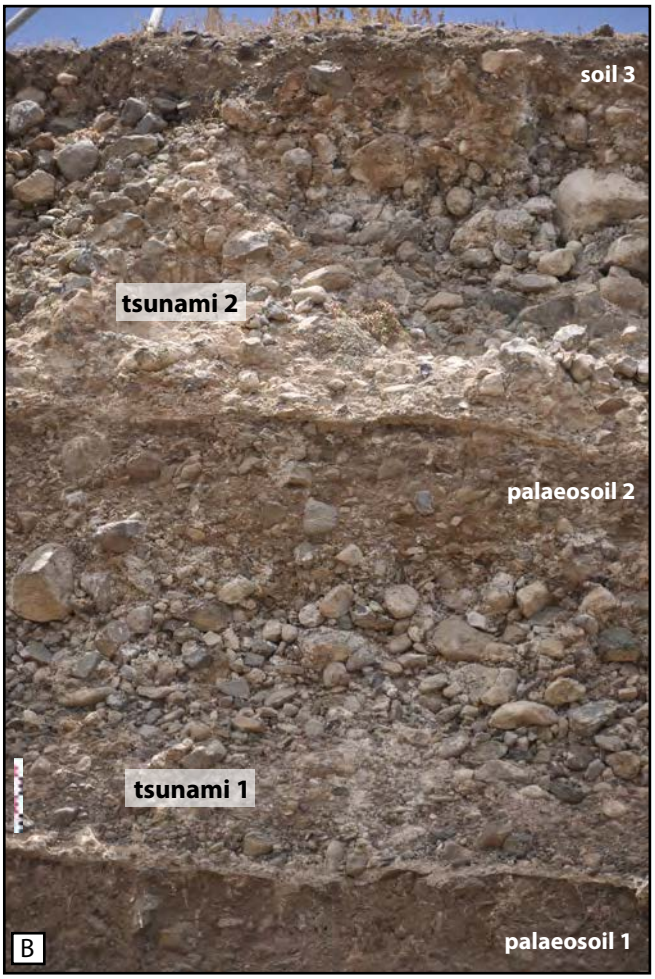
soil 3
tsunami 2
palaeosoil 2
tsunami 1
palaeosoil 1
B
- calcrete +

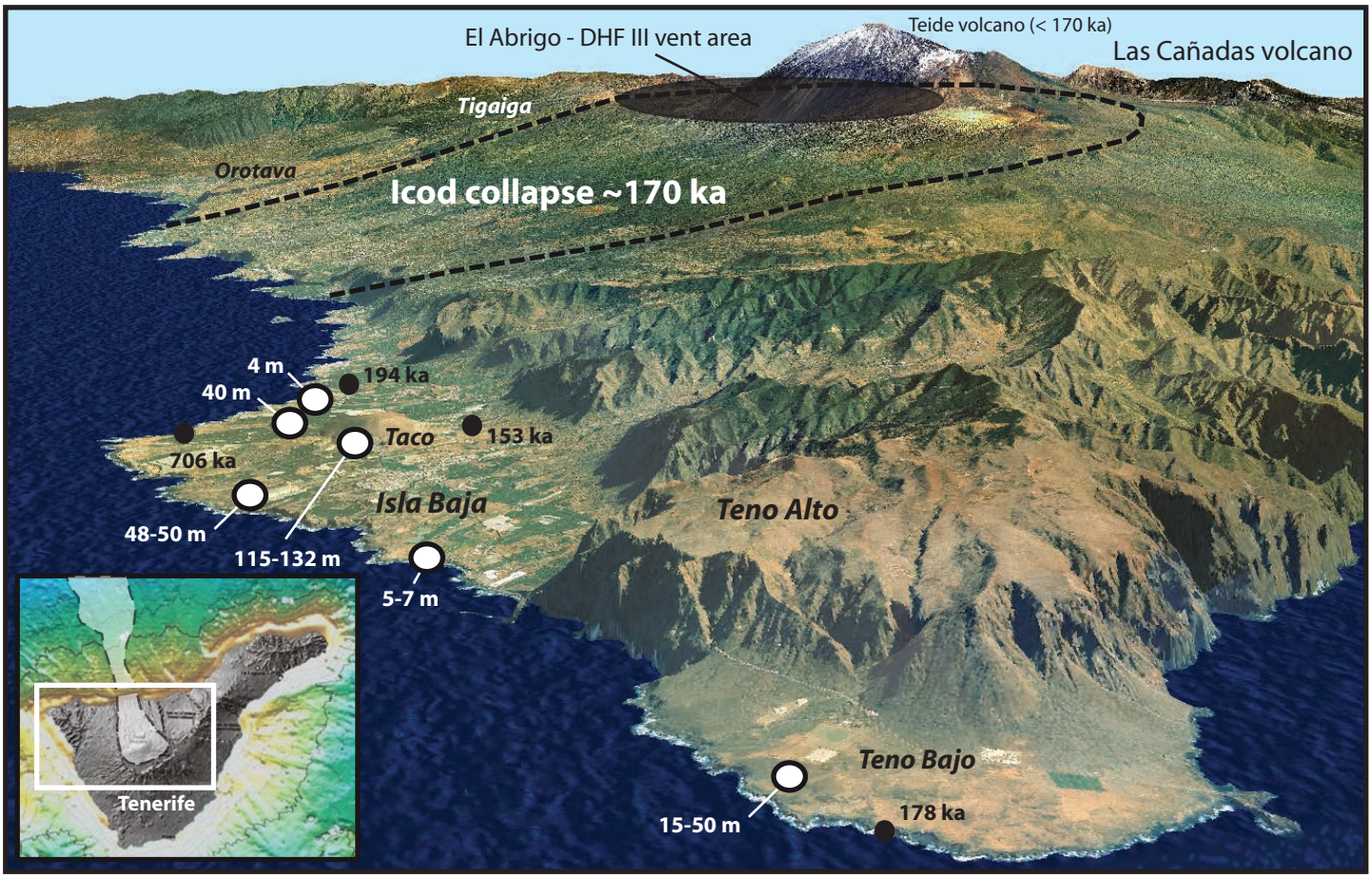
El Abrigo - DHF III vent area
Teide volcano (< 170 ka)
Las Cañadas volcano
Tigaiga
Orotava
Icod collapse ~170 ka
4 m
40 m
194 ka
Taco
153 ka
706 ka
48-50 m
115-132 m
Isla Baja
Teno Alto
5-7 m
Tenerife
Teno Bajo
15-50 m
178 ka

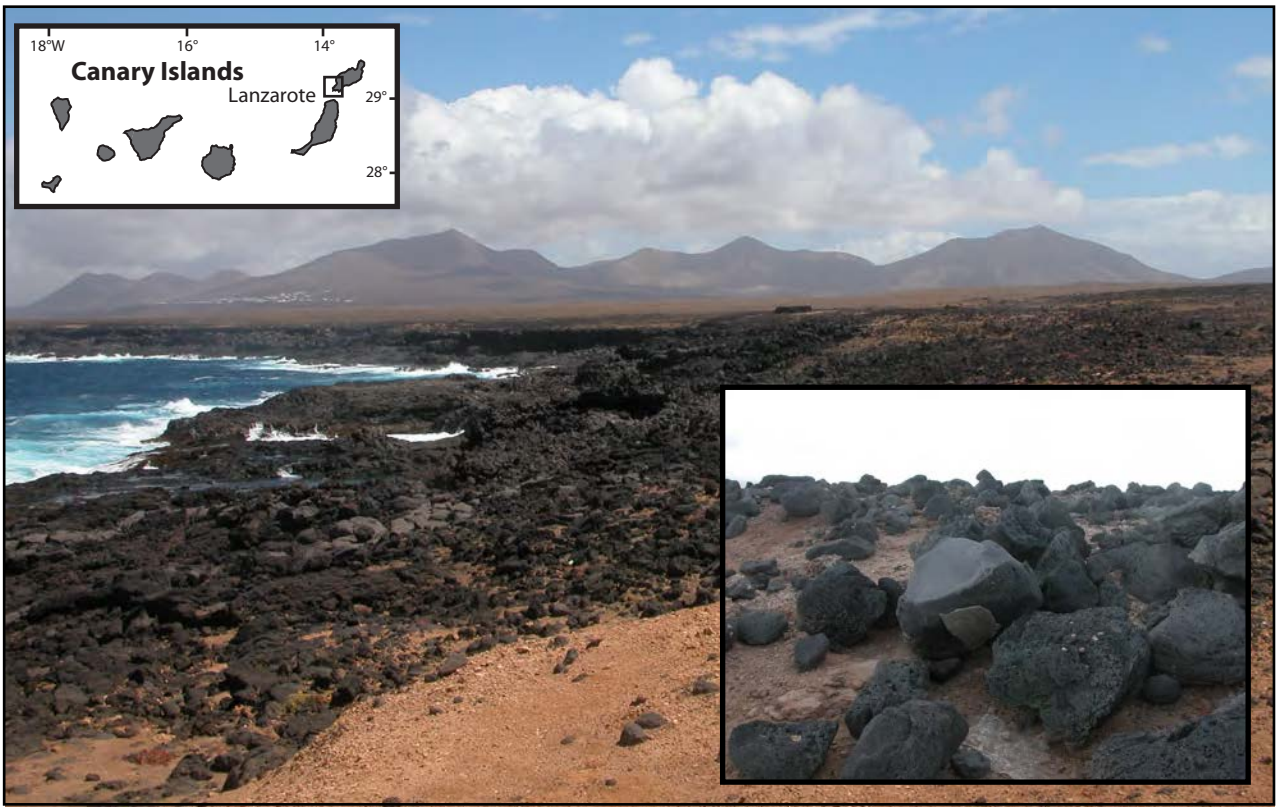
18°W
16°
14°
Canary Islands
Lanzarote
29°
28°

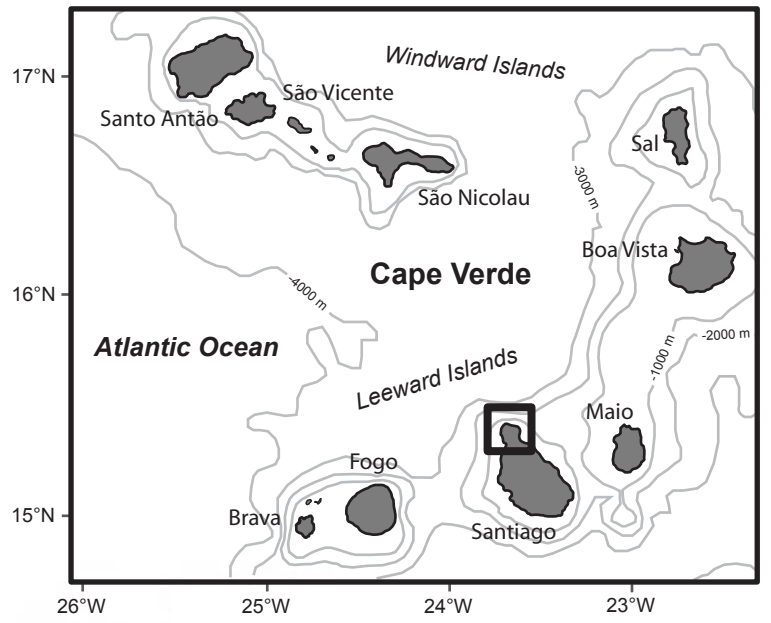
Windward Islands
São Vicente
Santo Antão
São Nicolau
Sal
Boa Vista
Cape Verde
Atlantic Ocean
Leeward Islands
Maio
Fogo
Brava
Santiago
-3000 m
-4000 m
-2000 m
-1000 m
17°N
16°N
15°N
26°W
25°W
24°W
23°W


B

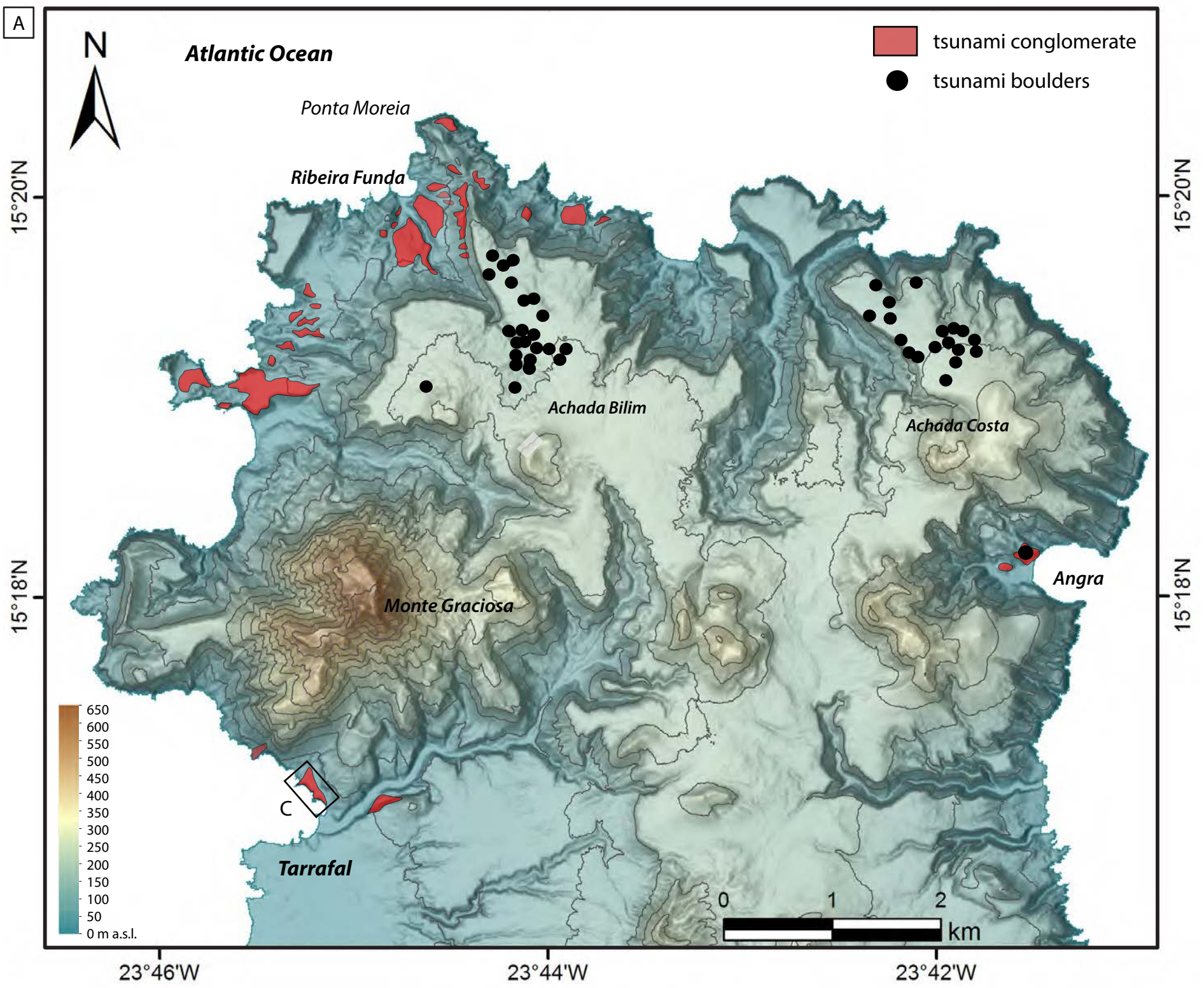
A
N
Atlantic Ocean
tsunami conglomerate
tsunami boulders
Ponta Moreia
Ribeira Funda
Achada Bilim
Achada Costa
Angra
Monte Graciosa
Tarrafal
C
650
600
550
500
450
400
350
300
250
200
150
100
50
0 m a.s.l.
0
1
2
km
15°20'N
15°18'N
23°46'W
23°44'W
23°42'W

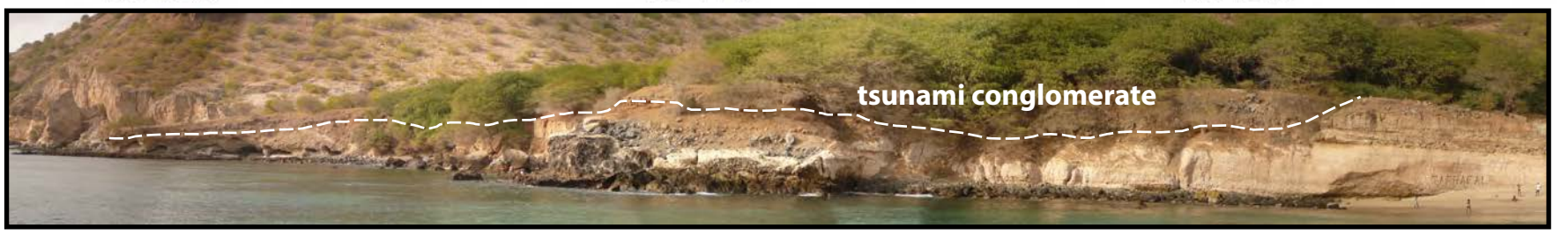
C
tsunami conglomerate


A


B


C


D

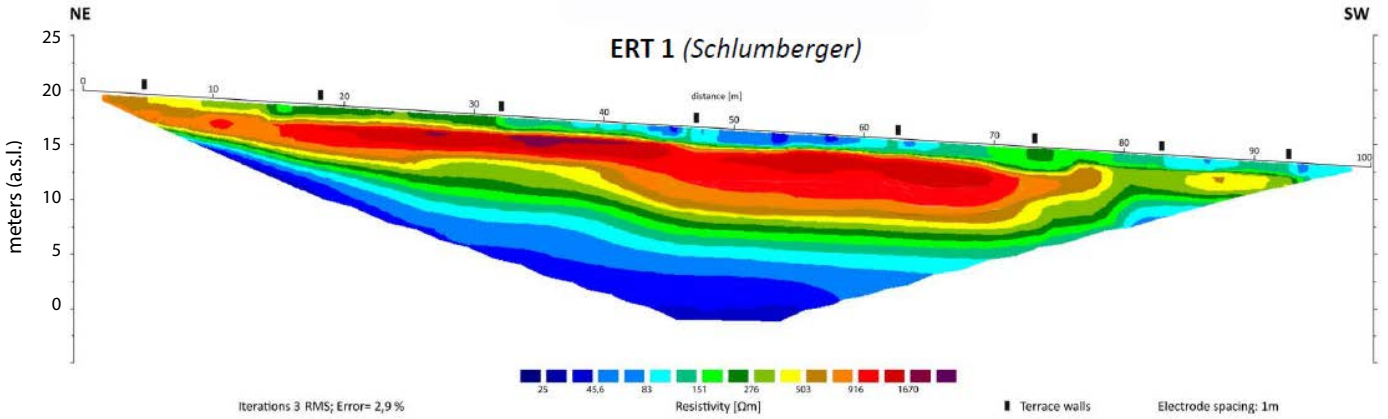
NE
SW
ERT 1 (Schlumberger)
meters (a.s.l.)
25
20
15
10
5
0
distance [m]
0
10
20
30
40
50
60
70
80
90
100
25
45,6
83
151
276
503
916
1670
Iterations 3 RMS; Error= 2,9 %
Resistivity [Ωm]
Terrace walls
Electrode spacing: 1m

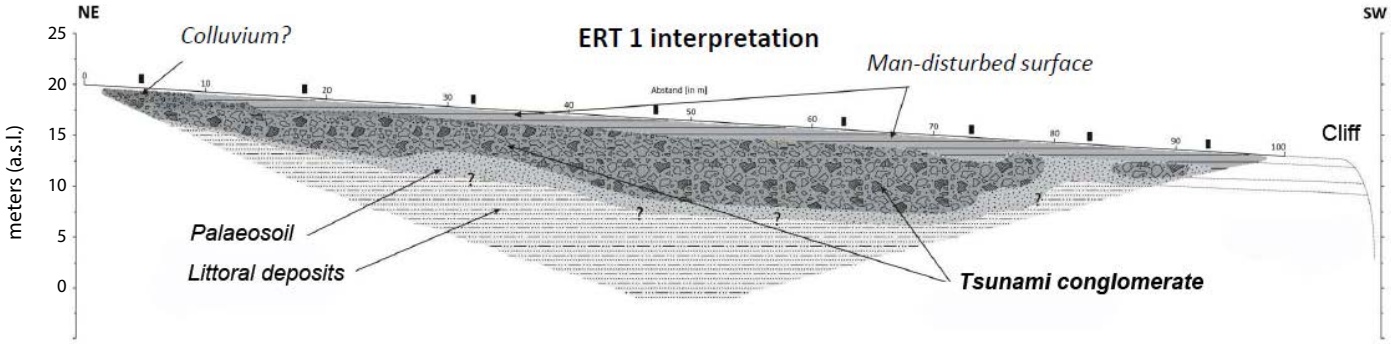
NE
SW
ERT 1 interpretation
meters (a.s.l.)
25
20
15
10
5
0
Colluvium?
Man-disturbed surface
Abstand [in m]
Cliff
Palaeosoil
Littoral deposits
Tsunami conglomerate
?

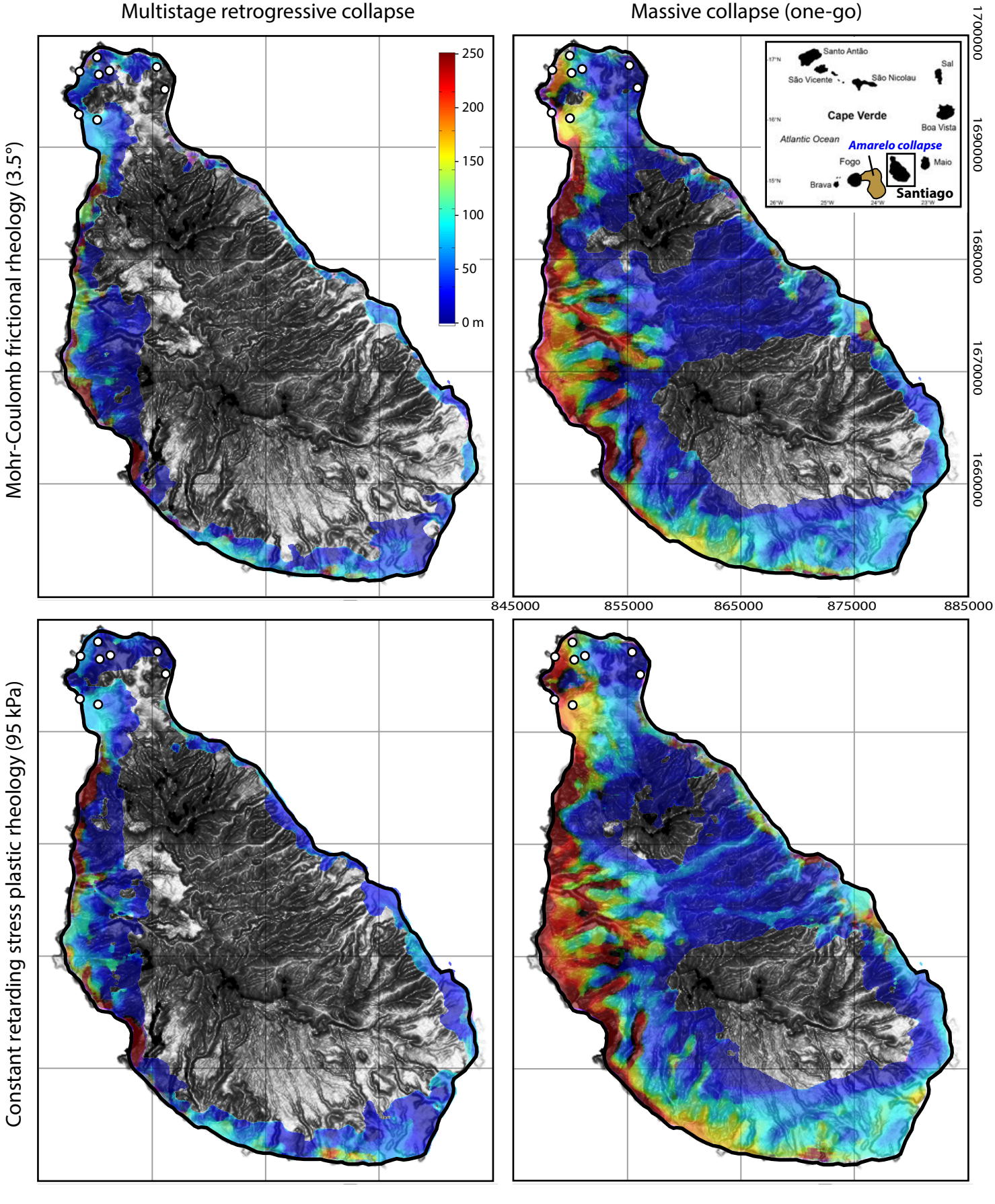
Multistage retrogressive collapse
Massive collapse (one-go)
Mohr-Coulomb frictional rheology (3.5°)
Constant retarding stress plastic rheology (95 kPa)
250
200
150
100
50
0 m
Santo Antão
Sal
São Vicente
São Nicolau
Cape Verde
Boa Vista
Atlantic Ocean
Amarelo collapse
Fogo
Maio
Brava
Santiago
1700000
1690000
1680000
1670000
1660000
845000
855000
865000
875000
885000

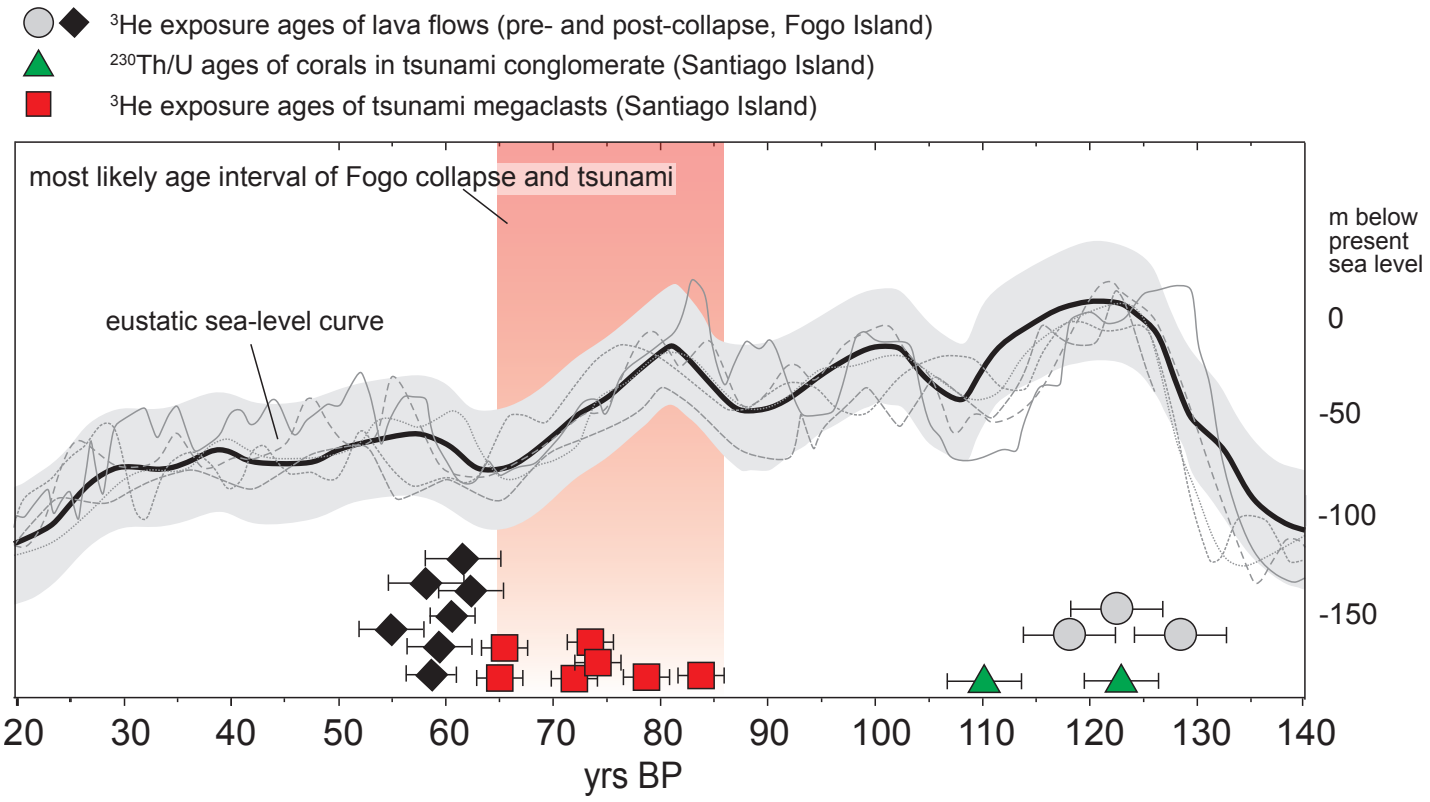
3He exposure ages of lava flows (pre- and post-collapse, Fogo Island)
230Th/U ages of corals in tsunami conglomerate (Santiago Island)
3He exposure ages of tsunami megaclasts (Santiago Island)
most likely age interval of Fogo collapse and tsunami
eustatic sea-level curve
m below present sea level
0
-50
-100
-150
20
30
40
50
60
70
80
90
100
110
120
130
140
yrs BP

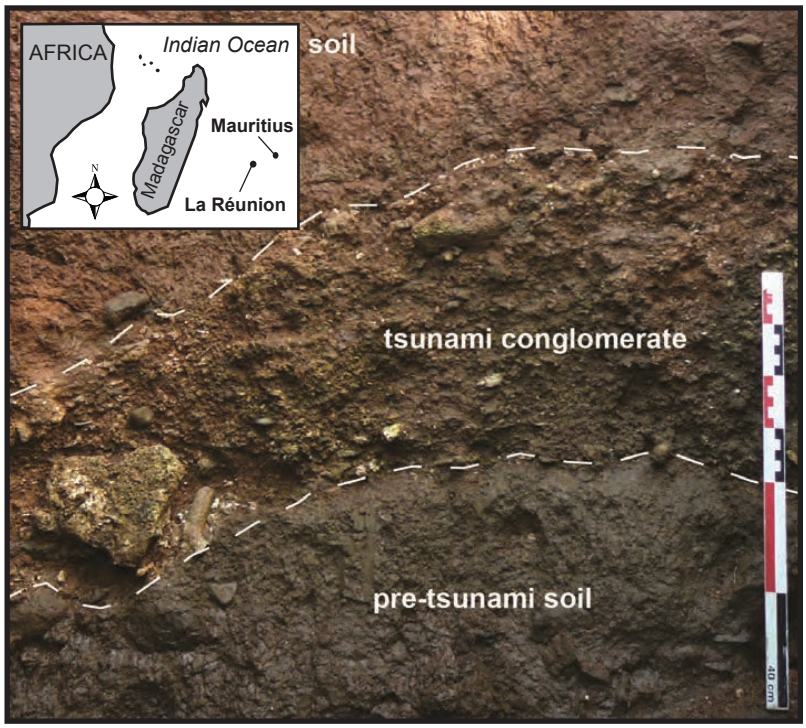
AFRICA
Indian Ocean
Madagascar
Mauritius
La Réunion
N
soil
tsunami conglomerate
pre-tsunami soil
40 cm

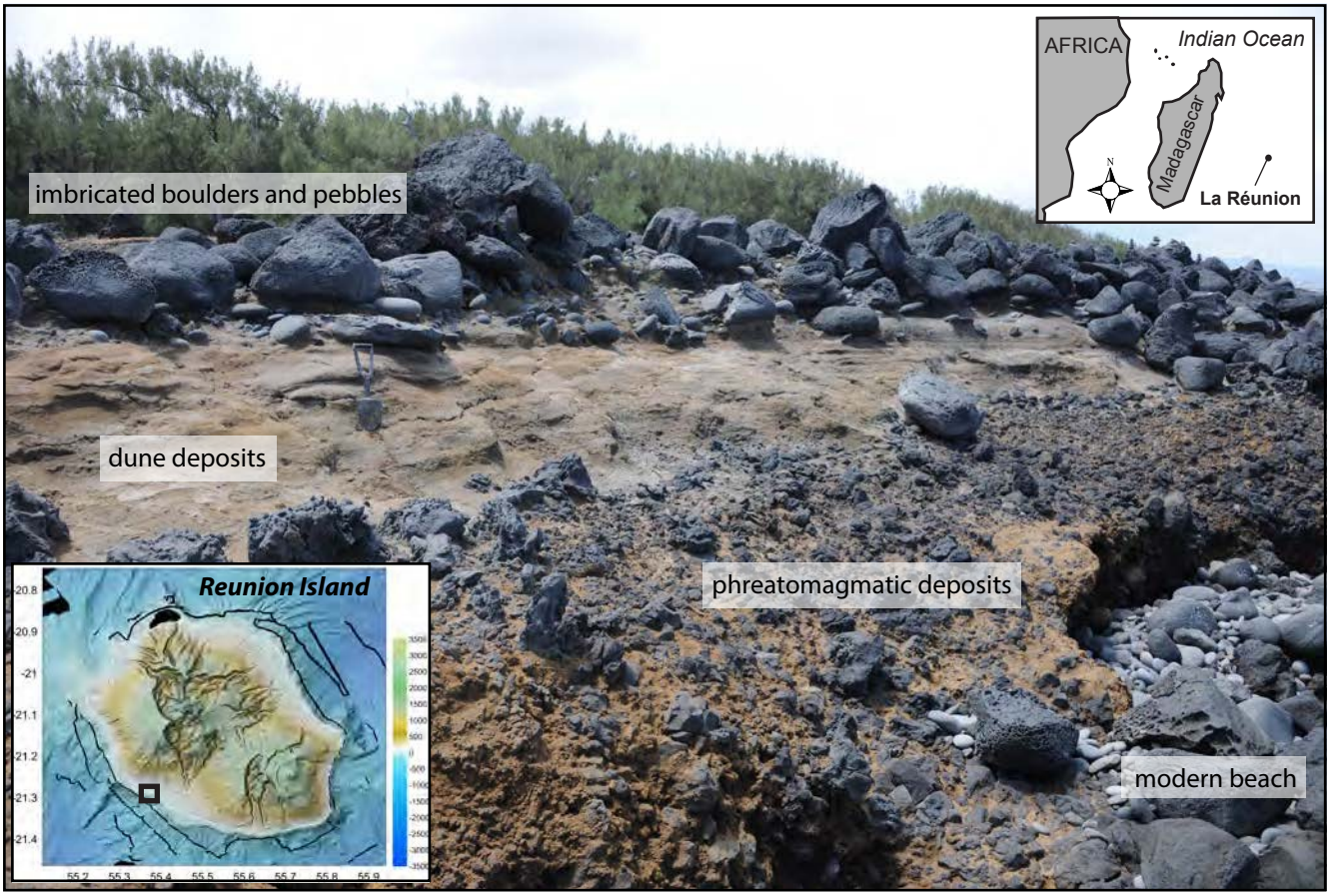
AFRICA
Indian Ocean
Madagascar
N
La Réunion
imbricated boulders and pebbles
dune deposits
phreatomagmatic deposits
modern beach
Reunion Island
20.8
20.9
-21
21.1
21.2
21.3
21.4

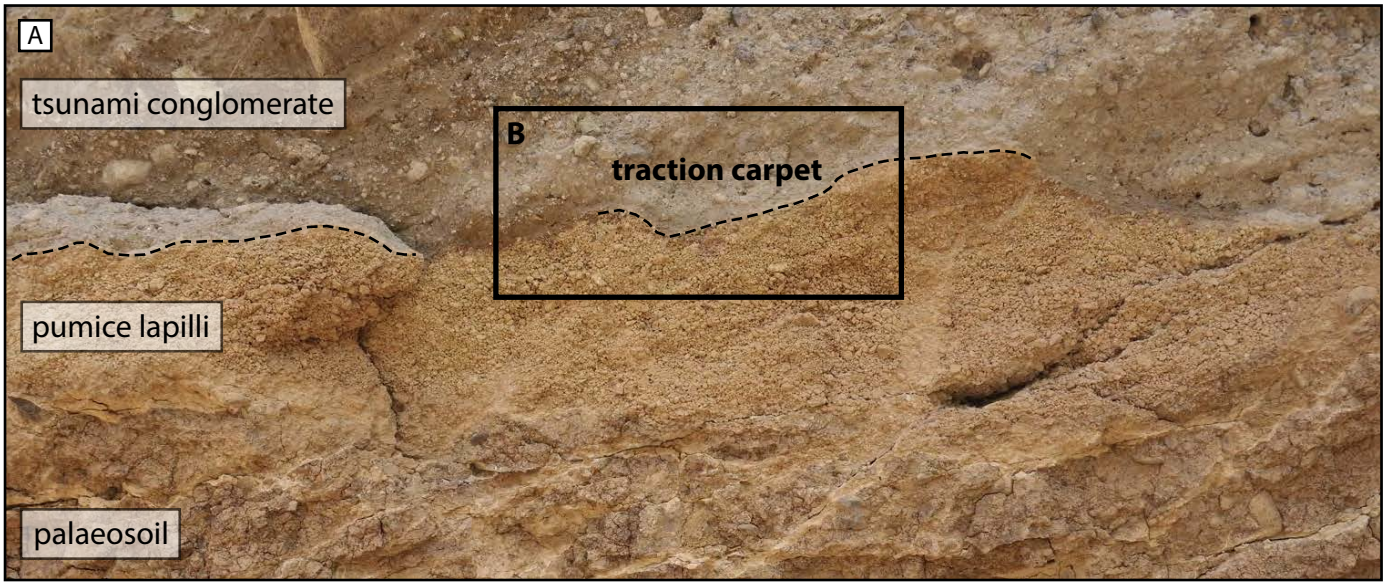
A
tsunami conglomerate
B
traction carpet
pumice lapilli
palaeosoil

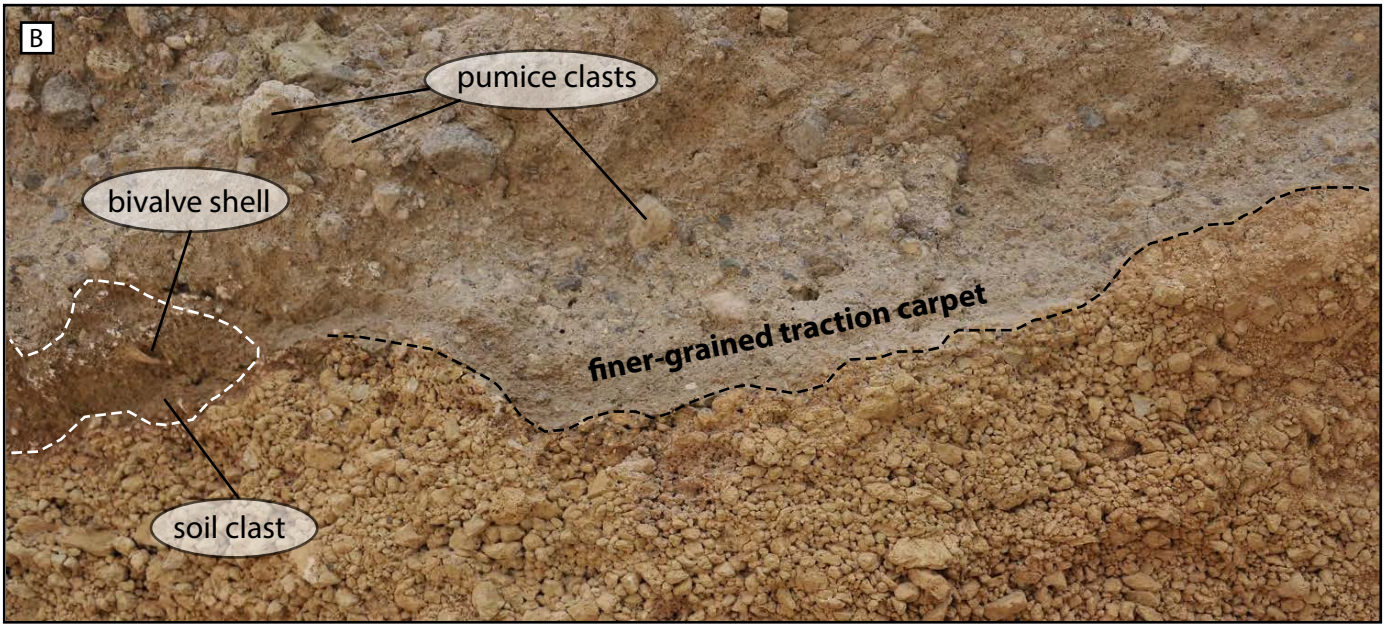
B
pumice clasts
bivalve shell
finer-grained traction carpet
soil clast

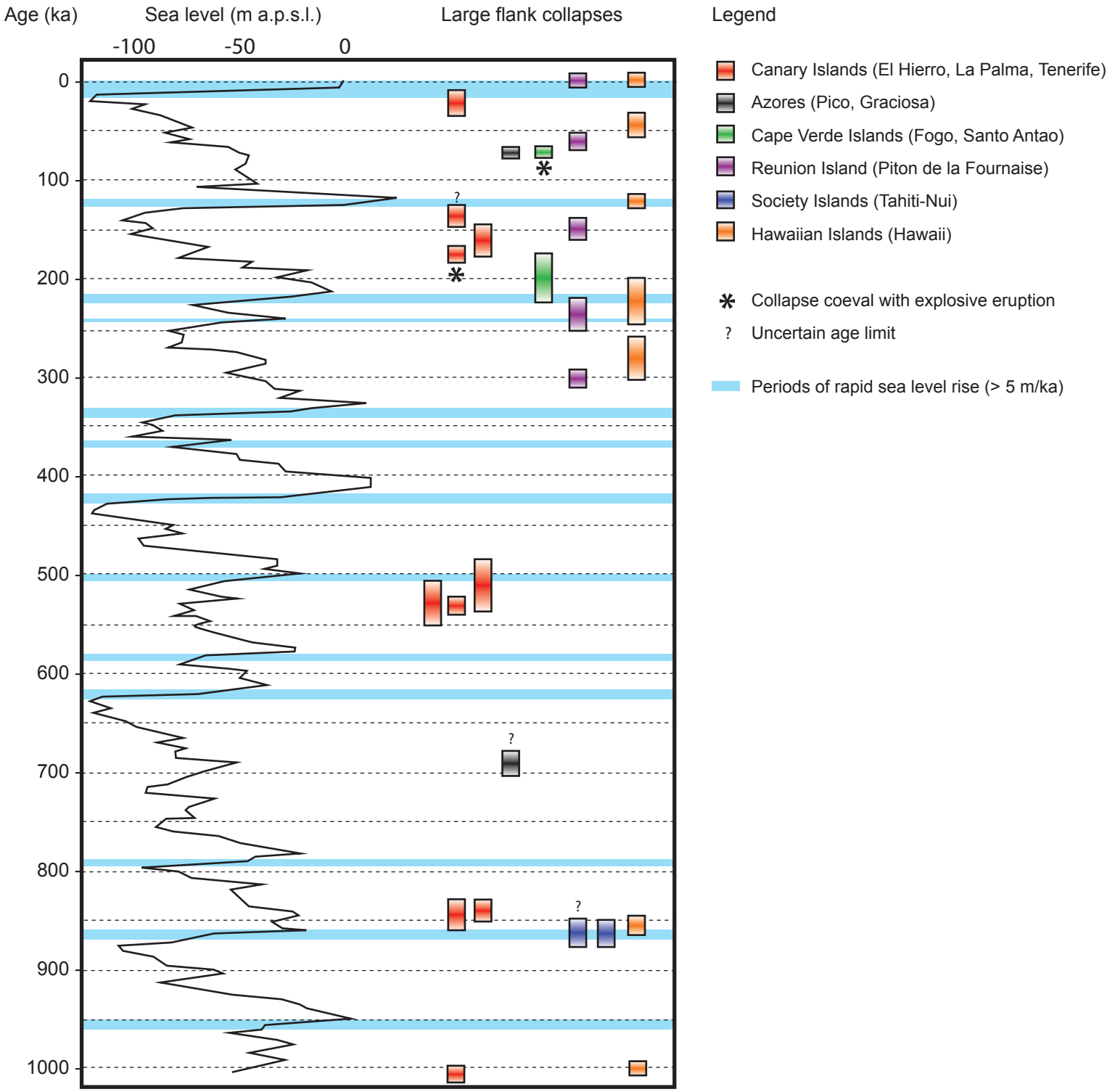
Age (ka)
Sea level (m a.p.s.l.)
-100
-50
0
0
100
200
300
400
500
600
700
800
900
1000
Large flank collapses
Legend
Canary Islands (El Hierro, La Palma, Tenerife)
Azores (Pico, Graciosa)
Cape Verde Islands (Fogo, Santo Antao)
Reunion Island (Piton de la Fournaise)
Society Islands (Tahiti-Nui)
Hawaiian Islands (Hawaii)
Collapse coeval with explosive eruption
Uncertain age limit
Periods of rapid sea level rise (> 5 m/ka)

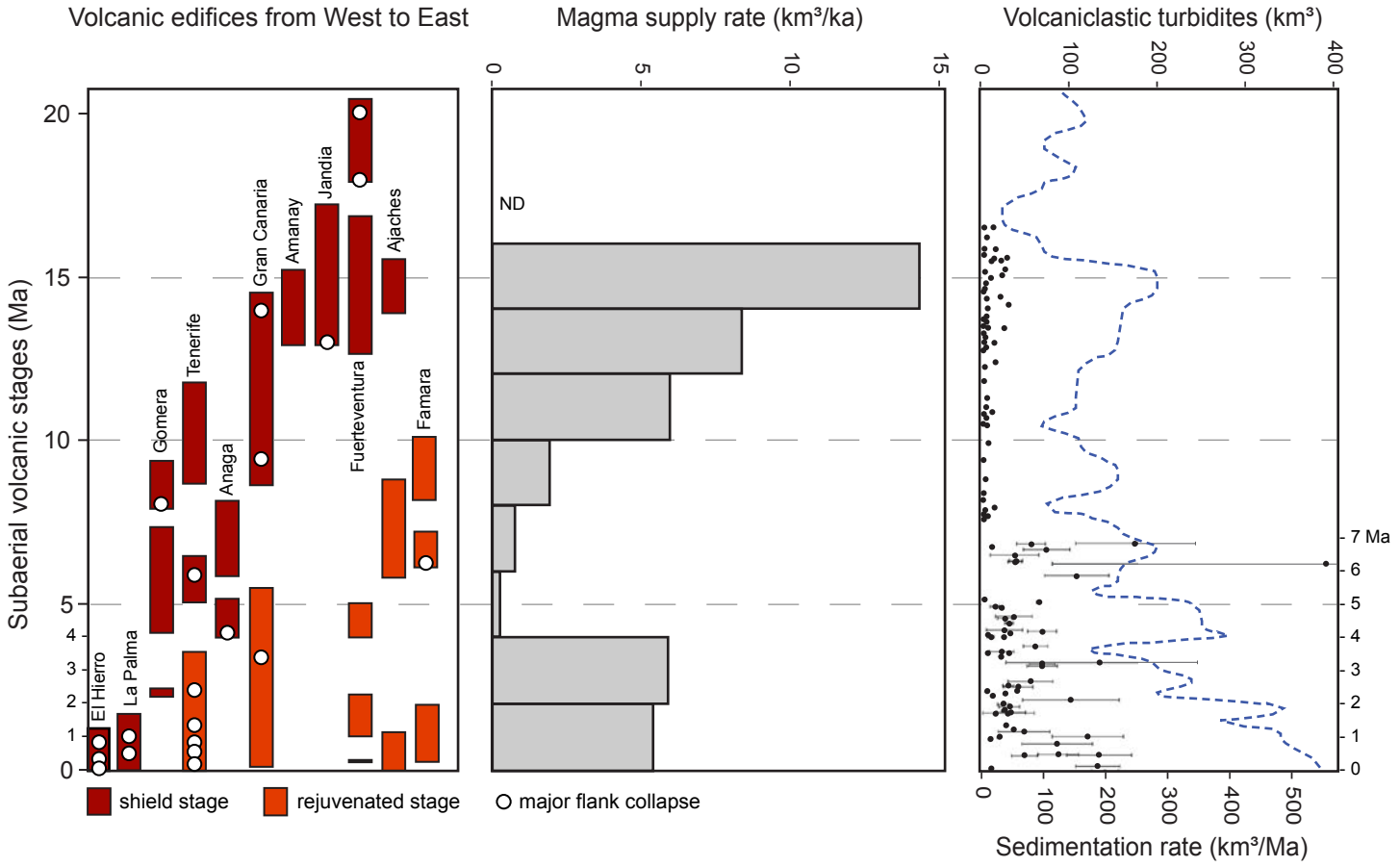
Volcanic edifices from West to East
Magma supply rate (km³/ka)
Volcaniclastic turbidites (km³)
Subaerial volcanic stages (Ma)
El Hierro
La Palma
Gomera
Tenerife
Anaga
Gran Canaria
Amanay
Jandia
Fuerteventura
Ajaches
Famara
ND
7 Ma
Sedimentation rate (km³/Ma)
shield stage
rejuvenated stage
major flank collapse

Table 1 – Characteristics of tsunami conglomerates and gravels. References are listed in chronological order of publication. 1: Moore & Moore (1984); 2: Moore & Moore (1988); 3: Moore et al. (1994); 4: Shiki & Yamazaki (1996); 5: Felton et al. (2000); 6: Moore (2000); 7: Felton et al. (2004); 8: Le Roux et al. (2004); 9: McMurtry et al. (2004); 10: Cantalamessa & Di Celma (2005); 11: Schnyder et al. (2005); 12: Le Roux & Vargas (2005); 13: Fujino et al. (2006); 14: Perez-Torrado et al. (2006); 15: Meco (2008); 16: Paris et al. (2010); 17: Paris et al. (2011); 18: Paris et al. (2013); 19: Navarrete et al. (2014); 20: Ramalho et al. (2015); 21: Paris et al. (2017).

Characteristics	Observations	References
Morphology		
Geometry	Patchy distribution, often lenticular	1, 4, 9, 14, 20, 21
	Well-defined unit exposed along cliffs	8, 10, 17
	Ridges	2
Thickness	*Typically 0.5-5 m*	
	Landward thinning	1, 14, 18, 20
	Landward thickening	17
Structure		
Organisation	Subunits (often 2 subunits) with poor lateral continuity	1, 9, 14, 17, 20
	Fining upward sequence of subunits	9, 10, 13, 14, 19, 20, 21
	Coarsening upward sequence of subunits	1, 3
	Erosional discontinuities between subunits (scour-and-fill)	1, 13, 14, 21
	Lenticular fine-grained (sand, small pebbles) interbeds	13, 17, 20
Bedforms	Obscurely bedded (crude lamination)	2, 8, 21
	Parallel lamination	4, 19
	Cross-lamination	8, 19
	Unbedded	3, 17
Basal contact	Fine-grained traction carpet	8, 17, 21
	Downward injected clastic dykes	3, 4, 8, 12, 17, 21
	Carbonate veins filling cracks and joints	1, 3
	Erosive contact, truncated substratum	4, 5, 11, 13, 14, 17, 18
	Irregular contact (no clear discontinuity)	20
Texture		
Grain size	*Pebble-to-boulder size clasts*	
	Clay-to-sand matrix	3
	Sand-to-gravel matrix	14, 17, 18
	Coarse sand matrix	10, 19
Vertical grading	Ungraded	3, 9, 10, 17, 21
	Ungraded to inversely graded	2, 8, 14, 17
	Inverse grading at the base	4, 9
	Normal grading at the top	10
	Inversely graded lenses	21
	Inverse grading turning to normal grading	10
Horizontal grading	Landward fining	1, 6, 14, 18, 21

	(*often difficult to evaluate due to limited exposure*)	
Sorting	Poorly sorted to very-poorly sorted	3, 18, 20
	Moderately to very-poorly sorted	10, 17
	Lower subunit very poorly sorted, upper subunit poorly sorted	14
Fabric type	All subunits clast-supported	4, 13, 14, 17
	Lower clast-supported subunit, upper matrix-supported subunit	1, 9, 21
	Uppermost matrix-supported subunit (normally graded)	10
	Matrix-supported	19
Fabric orientation	Landward	2, 20
	Landward (uprush subunits) and seaward (backwash subunits)	13, 14
	Fabric orientation differs from one subunit to another	17
Clast shape	Angular to rounded (source-dependent)	1, 9, 14, 17
	Roundness decreasing landward	14, 20
Composition		
Matrix	*Heterogeneous composition (locally-derived rocks and bioclasts)*	
	Carbonate-cemented (calcrete)	1, 14, 17
Clasts	*Heterogeneous composition (locally-derived rocks)*	
	Rip-up clasts of the substratum (e.g. soil)	4, 7, 8, 11, 14, 20, 21
	Organic debris (wood, plants)	11, 13
Bioclasts	*Fragments of bivalves, gastropods, corals, coralline algae, bryozoans, serpulids, urchins, foraminifers and diatoms*	
	Corals and coralline algae are not in a growth position	1, 3, 9, 14
	Degree of fragmentation of shells increasing landward	14
	Benthic foraminifers (littoral, rare deep water), no planktonic species	9
	Mixing of littoral to infralittoral mollusc species	1
	Mixing of circalittoral to terrestrial mollusc species	15
	Dominant infralittoral and circalittoral fauna	21
	Mixing of marine and terrestrial vertebrates	11
Variations of bioclast abundance	Abundance decreasing landward	20, 21
	Upper subunits enriched in bioclasts	9, 14
	Lower subunits enriched in bioclasts	1, 3, 17
	Enriched zones (finer-grained facies)	17
	Subunits or lenses without bioclasts	3, 9, 17